ELSEVIER

Chemical Geology 236 (2007) 42–64

CHEMICAL GEOLOGY
INCLUDING
ISOTOPE GEOSCIENCE

www.elsevier.com/locate/chemgeo

Petrogenesis of Carboniferous adakites and Nb-enriched arc basalts in the Alataw area, northern Tianshan Range (western China): Implications for Phanerozoic crustal growth in the Central Asia orogenic belt

Qiang Wang [a], Derek A. Wyman [b,*], Zhen-Hua Zhao [a], Ji-Feng Xu [a], Zheng-Hua Bai [a], Xiao-Lin Xiong [a], Tong-Mo Dai [a], Chao-Feng Li [c], Zhu-Yin Chu [c]

[a] *Key Laboratory of Isotope Geochronology and Geochemistry, Guangzhou Institute of Geochemistry, Chinese Academy of Sciences, Guangzhou 510640, PR China*

[b] *School of Geosciences, Division of Geology and Geophysics, The University of Sydney, NSW 2006, Australia*

[c] *Institute of Geology and Geophysics, Chinese Academy of Sciences, Beijing 100029, PR China*

Received 27 October 2005; received in revised form 18 August 2006; accepted 22 August 2006

Editor: R.L. Rudnick

Abstract

Carboniferous volcanic rocks in the Alataw area, Northern Tianshan Range (Xinjiang), consist of early Carboniferous (ca. 320 Ma) adakites and Nb-enriched arc basalts and basaltic andesites (NEBs), and late Carboniferous (ca. 306–310 Ma) mainly high-K calc-alkaline andesites, dacites and rhyolites. The adakites are calc-alkaline, and characterized by high Na_2O/K_2O (1.52–3.32) ratios, negligible to positive Eu anomalies, strong depletion of heavy rare earth elements (e.g., Yb = 0.74–1.47 ppm) and Y (6.7–14.9 ppm), positive Sr and Ba but negative Nb and Ti anomalies, and relatively constant $\varepsilon_{Nd}(T)$ values (+3.4–+6.6) and $(^{87}Sr/^{86}Sr)_i$ ratios (0.7035–0.7042). Some andesitic and dacitic adakite samples exhibit high MgO contents similar to magnesian andesites. The NEBs are sodium-rich ($Na_2O/K_2O = 2.03–8.06$), and differ from the vast majority of arc basalts in their higher Nb, Zr, TiO_2 and P_2O_5 contents and Nb/Th, Nb/La and Nb/U ratios, and minor negative to positive anomalies in Ba, Nb, Sr, Zr and Ti. They have the highest $\varepsilon_{Nd}(T)$ values (+6.4–+11.6) but varying $(^{87}Sr/^{86}Sr)_i$ ratios (0.7007–0.7063). The high-K calc-alkaline suite is similar to typical 'normal' arc volcanic rocks in terms of moderately fractionated rare earth abundance and distinctly negative Eu, Nb, Sr and Ti anomalies. They have $\varepsilon_{Nd}(T)$ values (+1.2–+6.4) and $(^{87}Sr/^{86}Sr)_i$ ratios (0.7018–0.7059). Geochemically, they are similar to coeval I-type granitoids in the Alataw area. Given the presence of early Carboniferous ophiolites in the Northern Tianshan Range, and the isotopically inappropriate compositions of Proterozoic metamorphic basement in the Alataw area, we argue that the Alataw adakites were most probably related to the melting of young subducted crust of the Northern Tianshan Ocean. The NEBs likely originated from mantle wedge peridotites metasomatized by adakites and minor slab-derived fluids. The later high-K calc alkaline suite was generated by AFC processes that acted on melts derived from a mantle wedge metasomatized by hydrous fluids. The larger range of isotopic compositions exhibited by both the NEB and high-K suite, relative to the adakites, suggests that the mantle wedge was heterogeneous prior to slab- or fluid-mediated metasomatism.

* Corresponding author. Tel.: +61 2 9351 2924; fax: +61 2 9351 0184.
E-mail address: dwyman@geosci.usyd.edu.au (D.A. Wyman).

0009-2541/$ - see front matter
doi:10.1016/j.chemgeo.2006.08.013

Continental crustal growth of the Central Asian orogenic belt was dominated by contributions of the juvenile materials from the depleted mantle prior to 270 Ma and possibly afterwards. The results of this study suggest that other Carboniferous Nb-enriched basalts in the Tianshan Range were generated by subduction processes rather than by intraplate tectonics as previously proposed.

Keywords: Adakite; Nb-enriched basalts; Slab melting; Mantle metasomatism; Crust growth; Tianshan

1. Introduction

The Central Asian orogenic belt (CAOB), also known as the Altaid Tectonic Collage (Sengör et al., 1993), represents one of the most important sites of juvenile crustal growth during the Phanerozoic (Sengör et al., 1993; Jahn et al., 2000a,b). However, the mechanisms of continental crustal growth in the CAOB remain the subject of debate. Sengör et al. (1993) suggested that CAOB grew by 5.3 million square kilometers during the Palaeozoic, with nearly half of this growth being derived from the mantle by subduction accretion and arc collision. This model is supported by the presence of ophiolites with ages ranging from Neoproterozoic to late Paleozoic (e.g., Coleman, 1989; Xiao et al., 1992; He et al., 1994; Zhou et al., 2001; Pfander et al., 2002; Gao and Klemd, 2003; Xiao et al., 2003; Xu et al., 2003; Liu and Fei, 2006) and occurrences of Paleozoic arc-style magmatic rocks (e.g., Chen et al., 2000a; Heinhorst et al., 2000; Hu et al., 2000a). Conversely, many researchers argue that massive Phanerozoic CAOB granitoids with positive ε_{Nd} values are A-type granites generated by extensive basalt underplating in a post-orogenic or an intraplate extensional setting (e.g., Zhao et al., 1996; Han et al., 1997; Jahn et al., 2000a,b; Liu, 2002; Wu et al., 2000, 2002; Liu and Fei, 2006). Moreover, some recent studies indicate that Late Paleozoic plume activity provided the heat required to generate the large amounts of granites and associated volcanic rocks in the CAOB (Xia et al., 2004a; Zhou et al., 2004).

The origin of Carboniferous volcanic rocks of the Tianshan Range in the western CAOB has been part of the larger debate concerning the orogenic belt. They have been interpreted as either part of a Carboniferous arc (Windley et al., 1990; Xiao et al., 1992; Hsü et al., 1994; Chen et al., 1999; Li et al., 2002a; Zhao et al., 2003; Zhou et al., 2004; Liu and Fei, 2006) or as the product of a rift setting (e.g., Che et al., 1996; Gu et al., 2000; Xia et al., 2004a,b). Our study presents new geochronological data that provide geodynamic context for the Alataw volcanism during evolution of the Tianshan Range. New geochemical data establishes that volcanic rocks in the Alataw area include a suite of Nb-enriched basalts (NEB) and coeval adakitic dacitic to rhyolitic adakites and a suite of mainly high-K calc-alkaline andesites, dacites, and rhyolites. If the Alataw Carboniferous NEB-adakite suite is an example of the adakite metasomatic arc volcanic series (Defant and Kepezhinskas, 2001), then partial melting of subducted oceanic crust could represent an important additional continental crustal growth mechanism for Central Asia during the Paleozoic.

2. Geological setting

The Alataw Mountains are located in the north of the Bole–Wenquan area, Northwestern Xinjiang (Fig. 1), in the western part of the North Tianshan Range. Tectonically, they are in the northern part of the Yili–middle-Tianshan microplate, which is bounded to the northeast by the Junggar Plate and Northern Tianshan Variscan fold belt and to the south by the Southern middle-Tianshan Caledonian fold belt (Fig. 1). Paleontological data show that ophiolites in the Northern Tianshan Variscan fold belts are Carboniferous in age whereas those in the Southern middle-Tianshan Caledonian fold belts are Silurian–Devonian, in age (Xiao et al., 1992). Sensitive High-Resolution Ion Microprobe (SHRIMP) geochronology studies of zircons (Xu et al., 2006) confirm that the Bayinggou ophiolites in the Northern Tianshan Variscan fold belt were produced in the Early Carboniferous (325 ± 7 Ma).

Middle-Proterozoic basement, consisting of granitic gneisses and amphibolites, crops out in the southwestern part of the studied region (Chen et al., 2000b; Hu et al., 2000a) (Fig. 2). Early Paleozoic and Mesozoic strata are absent, but Late Paleozoic (Devonian and Carboniferous) and Cenozoic strata and sedimentary materials are widespread (Fig. 2). The eastern and western parts of the region are mainly covered by Devonian strata but Carboniferous sequences dominate in the central part of the study area. Devonian rocks include pelagic siliceous and silty mudstone, radiolarian mudstone and limestone in the lower strata, and littoral-neritic conglomerate, sandstone, siltstone, shale and limestone in the upper strata. Carboniferous rocks consist of sandstone,

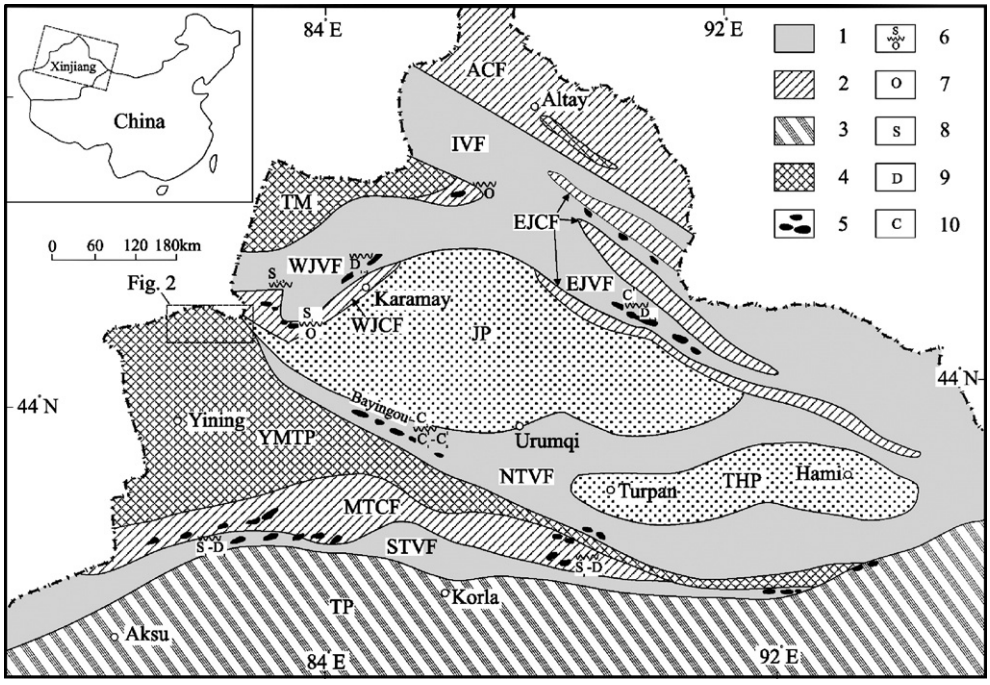

Fig. 1. Schematic map of tectonic units of Northern Xinjiang (Xiao et al., 1992) 1—Late Paleozoic fold belts; 2—Early-middle Paleozoic fold belts; 3—Early Proterozoic basements; 4—Late Proterozoic basements; 5—Ophiolitic fragments; 6—Forming and emplacing time of ophiolite; 7—Ordovician; 8—Silurian; 9—Devonian; 10—Carboniferous. ACF—Altay Caledonian fold belt; IVF—Irtysh Variscan fold belt; TM—Tacheng massif; WJVF—West-Junggar Variscan fold belt; WJCF—West-Junggar Caledonian fold belt; EJVF—East-Junggar Variscan fold belt; EJCF—East-Junggar Caledonian fold belt; JP—Junggar Plate; THB—Tulufan–HamiPlate; NTVF—Northern Tianshan Variscan fold belt; YMTP—Yili–middle-Tianshan Plate; STVF—Southern-Tianshan Variscan fold belt; MTCF—Southern middle-Tianshan Caledonian fold belt; TP—Tarim Paleoplate.

siltstone, limestone, and some volcanic rocks, including basalt, andesite, dacite and rhyolite. The volcanic rocks mainly outcrop in the Halatulukegou area and along the west side of Aibi Lake (Fig. 2). In the Halatulukegou area, the volcanic rocks are principally dacites, rhyolites, andesites, volcanic breccias, and tuffaceous

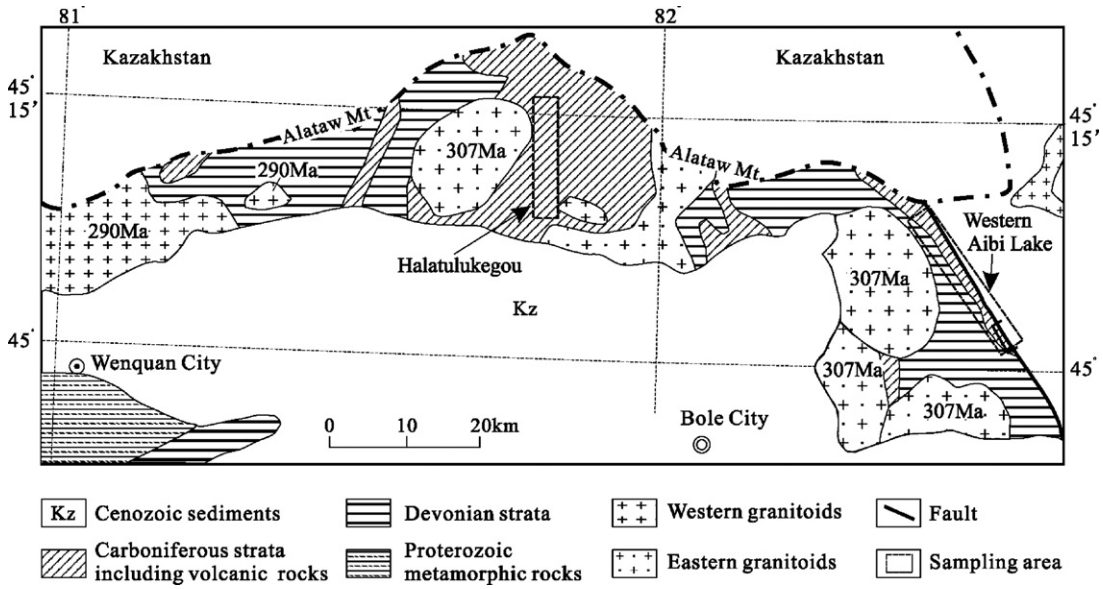

Fig. 2. The geological map of the Alataw Mountains in Northern Xinjiang (after Chen et al. (2000b)).

breccias. In the western Aibi Lake area, the volcanic rocks mainly comprise basalts, tuffaceous andesites, dacites and breccias. Paleontological fossils from sedimentary rocks associated with the volcanic rocks in both areas corroborate that the volcanic rocks erupted in the Carboniferous (Man, 1990).

Many granitoid intrusions crop out along the southern slope of the Alataw Mountains where they were emplaced into Devonian and Carboniferous sedimentary and volcanic rocks (Fig. 2). Based on their age, petrology, geochemistry and metallogenic characteristics, they can be divided into two groups. The eastern I-type granitoids consist of Late Carboniferous (307±3 Ma) hornblende-bearing granodiorites and granites (Chen et al., 1994, 2000b The western S-type granitoids are early Permian (290±3 Ma) two-mica granites with minor garnet. Metallogenic associations also serve to distinguish the two suites. Although genetically related ore deposits have not been found in the eastern granitoids, minor copper and gold mineralization is observed at or near the contacts of some intrusions. In contrast, the western granites are associated with small tin and tungsten ore deposits (Chen et al., 1994, 2000b).

3. Analytical methods

Samples from the Alataw volcanic rocks were initially examined by optical microscopy; unaltered or the least-altered samples were selected for further analysis.

Selected relatively fresh whole rock chips were ultrasonically cleaned in distilled water with <5% HNO_3 and distilled water, successively, and then dried and handpicked to remove visible contamination. The rock chips were wrapped in Sn foil and sealed in 6-mm-ID evacuated quartz-glass vials together with ZBH-25

Table 1
Summary of Argon isotopic results

T(°C)	$^{40}Ar/^{36}Ar$	$^{39}Ar/^{36}Ar$	$^{37}Ar/^{39}Ar$	F	$^{39}Ar(\times 10^{-12}$ mol)	^{39}Ar(%)	$^{*40}Ar$(%)	Age (Ma)	1σ (Ma)
WXT740, adakite (J=0.004078, W=0.3586 g)									
350	480.9570	3.6007	4.1397	51.5062	0.0086	0.98	38.56	343.9	40.4
480	675.8920	8.0449	7.8097	47.2835	0.0399	4.52	56.27	318.1	7.0
600	732.3420	9.1181	4.6364	47.9093	0.0676	7.74	59.64	321.9	4.6
750	637.4029	7.2546	3.0163	47.1289	0.1080	12.24	53.63	317.1	3.6
850	653.1830	7.4421	2.2825	48.0623	0.1348	15.28	54.75	322.9	2.9
980	741.5307	9.2202	2.0998	48.3755	0.1647	18.67	60.14	324.8	2.7
1120	784.6522	10.3085	1.5720	47.4514	0.2142	24.28	62.33	319.1	2.1
1200	737.5966	9.4879	1.9906	46.5956	0.1182	13.40	59.93	313.8	3.2
1250	743.4740	9.3864	12.5734	47.7260	0.0179	2.03	60.25	320.8	24.9
1350	763.3552	22.0149	24.0095	49.9653	0.0083	0.94	61.28	334.5	42.9
WXT721, Nb-enriched arc basalt (J=0.004080, W=0.2770 g)									
350	449.4980	3.6539	7.1390	42.1457	0.0048	0.98	34.26	286.2	73.7
480	575.0146	5.9898	12.6911	46.6654	0.0223	4.58	48.61	314.4	12.9
600	651.1679	7.7164	7.9768	46.0923	0.0372	7.72	54.61	310.8	8.5
750	640.1646	7.3337	5.8023	46.9972	0.0547	11.24	53.83	316.4	7.2
850	660.1877	7.7264	3.9884	47.2005	0.0744	15.28	55.23	317.7	5.2
980	675.2742	7.9521	3.6822	47.7575	0.0897	18.44	56.23	321.1	5.1
1120	658.7160	7.4960	2.9803	48.4544	0.1126	23.14	55.13	325.4	4.1
1200	677.4500	8.2268	2.7885	46.4277	0.0765	15.71	56.37	312.9	5.0
1250	729.8890	8.8616	21.3984	49.0191	0.0101	2.08	59.51	328.9	45.0
1350	688.5440	51.6555	39.8219	52.6264	0.0044	0.91	57.08	350.9	84.3
WXT733, dacite (J=0.004075, W=0.2145 g)									
350	2310.3987	74.0964	12.2285	27.1929	0.0045	0.90	87.19	189.6	93.0
480	3377.1429	67.3702	13.9183	45.7419	0.0227	4.57	91.23	308.4	24.1
600	4384.2730	89.2686	8.8842	45.8030	0.0370	7.52	93.24	308.8	14.1
750	5139.1304	109.3693	5.8251	44.2869	0.0601	12.11	94.23	299.3	10.8
850	4624.4131	97.5746	4.7026	44.3652	0.0762	15.34	93.59	299.8	8.4
980	6221.0526	131.7377	3.9004	44.9799	0.0936	18.84	95.23	303.6	7.5
1120	7880.0000	164.8196	3.0879	46.0170	0.1204	24.25	96.23	310.1	7.0
1200	8242.5463	169.9887	4.9234	46.7504	0.0647	13.02	96.40	314.6	8.8
1250	10817.3617	214.2613	21.6405	49.1076	0.0128	2.57	97.25	329.1	51.3
1350	10236.6082	13.0486	39.1966	52.3465	0.0047	0.95	97.10	348.8	88.1

Table 2
Major (wt.%) and trace (ppm) elements concentrations of the Alataw volcanic rocks

Sample	WXT721	WXT727	XT012-1	XT012	XT014	XT017	P154-3	P201	WXT728	WXT729
Longitude	82°34′473″	82°34′468″	(a)	(a)	(a)	(a)	(b)	(b)	82°34′948″	82°34′832″
Latitude	45°02′317″	45°02′308″	(a)	(a)	(a)	(a)	(b)	(b)	45°01′938″	45°01′742″
Rocks	NEB	NEB	NEB	NEB	NEB	NEB	NEB	NEB	Rhyolite	Rhyolite
SiO_2	51.91	50.67	54.67	53.62	50.34	53.28	46.07	51.37	72.80	74.55
TiO_2	2.47	2.33	3.61	3.21	2.97	3.56	2.50	2.00	0.36	0.30
Al_2O_3	14.38	15.15	12.59	14.23	16.59	15.16	14.43	15.27	12.99	11.62
Fe_2O_3	1.74	2.25	4.22	5.73	2.92	5.37	4.29	4.71	0.46	0.32
FeO	10.10	8.20	8.00	7.03	7.96	8.50	9.10	6.36	1.95	1.90
MnO	0.15	0.12	0.14	0.20	0.03	0.27	0.30	0.23	0.02	0.03
MgO	4.21	4.09	2.15	2.43	6.56	3.18	5.39	2.47	0.54	0.43
CaO	3.68	5.72	5.05	5.24	5.66	2.59	8.90	7.29	0.32	0.96
Na_2O	3.53	2.94	2.96	3.58	2.78	3.26	2.90	3.40	1.65	2.76
K_2O	1.07	1.02	1.46	1.59	0.59	1.41	0.36	0.55	6.82	4.95
P_2O_5	0.31	0.29	0.42	0.48	0.33	0.41	0.42	0.57	0.06	0.05
CO_2	1.81	2.83	2.83	0.00	0.00	1.35	1.88	2.76	0.34	0.74
H_2O	4.29	4.05	1.78	2.29	4.04	1.83	2.80	2.78	1.52	1.19
Σ	99.65	99.66	99.88	99.63	100.78	100.16	99.34	99.76	99.83	99.80
Na_2O/K_2O	3.30	2.88	2.03	2.25	4.71	2.32	8.06	6.18	0.24	0.56
$Mg^{\#}$	0.39	0.42	0.25	0.26	0.53	0.30	0.43	0.29	0.29	0.26
Sc	31.6	26.5	32.6	8.18	32.7	12.0			6.69	4.95
V	282	242	410	384	284	416			25.9	18.6
Cr	47.4	39.4	11.6	9.92	74.3	14.1			31.6	32.7
Co	31.9	35.8	33.4	29.4	38.9	32.2			3.26	3.16
Ni	64.5	38.6	9.14	5.29	56.7	9.60			10.5	9.01
Ga	20.3	19.6	24.3	23.0	19.2	22.0			17.7	14.0
Rb	18.2	19.0	25.5	3.22	4.64	4.00			138	106
Sr	905	633	368	293	409	354			63.1	108
Y	39.0	34.8	46.3	16.0	32.9	17.0	44	38	32.0	29.6
Zr	224	209	306	356	203	336	277	271	187	182
Nb	7.62	7.46	10.3	10.0	5.87	10.0	12.9	11.1	9.07	8.30
Ba	725	676	382	312	91.0	309	296	179	470	578
Hf	5.11	5.09	7.79	7.10	4.74	6.74			5.77	5.47
Ta	0.578	0.588	0.721	0.607	0.397	0.584			0.924	0.783
Pb	3.25	3.93	6.49	4.92	1.63	4.59			11.5	13.0
Th	0.976	1.63	2.41	0.381	0.709	0.428			9.62	9.02
U	0.297	0.490	0.608	0.673	0.226	0.579			2.05	2.02
La	10.3	10.7	17.4	8.33	9.34	7.49	11.3	17.5	24.0	23.5
Ce	27.1	28.1	43.6	23.82	25.7	21.7	31.56	42.13	53.5	50.7
Pr	4.03	4.04	6.58	3.91	4.09	3.61	5.27	6.42	6.13	5.87
Nd	20.7	19.9	30.1	19.18	20.1	17.78	24.70	26.59	24.8	24.7
Sm	5.81	5.39	7.43	4.81	5.10	4.60	6.95	6.8	5.23	5.18
Eu	2.08	1.83	2.50	1.55	1.69	1.53	2.38	1.82	0.863	0.860
Gd	6.50	5.49	8.58	5.22	6.20	5.00	7.98	7.92	5.05	5.05
Tb	0.990	0.911	1.45	0.981	1.04	0.94	1.41	1.24	0.823	0.785
Dy	6.21	5.79	8.61	6.09	6.19	5.84	8.47	6.96	5.11	4.89
Ho	1.46	1.37	1.74	1.32	1.25	1.26	1.80	1.5	1.16	1.14
Er	3.98	3.72	4.75	3.79	3.36	3.55	5.24	4.47	3.44	3.29
Tm	0.532	0.526	0.743	0.545	0.509	0.519	0.780	0.660	0.493	0.473
Yb	3.59	3.55	4.89	3.34	3.31	3.14	4.67	4.09	3.44	3.37
Lu	0.590	0.561	0.792	0.517	0.521	0.482	0.720	0.600	0.542	0.545

(a)These samples were collected in 1997 and their longitude and latitude were not given at that time; (b) P154-3 and P201 are from Chen et al. (2000b), and other samples are from this study. NEB: Nb-enriched basalts and basaltic andesites.
*Repeated samples.

WXT730	WXT731	WXT-732	WXT-733	XT-31	WXT-734	WXT751	WXT743	WXT746	WXT-736
82°35′496″	81°45′346″	81°45′948″	81°45′426″	(a)	81°45′465″	81°45′806″	81°46′321″	81°46′238″	81°45′767″
45°02′317″	45°14′346″	45°14′340″	45°14′301″	(a)	45°14′288″	45°11′604″	45°13′809″	45°13′311″	45°14′202″
Rhyolite	Dacite	Dacite	Dacite	Andesite	Dacite	Dacite	Rhyolite	Rhyolite	Adakite
73.80	66.09	67.95	65.91	61.98	65.74	66.05	75.63	77.05	62.73
0.35	0.92	0.74	0.89	1.02	0.92	0.88	0.31	0.29	0.57
12.93	14.60	14.15	14.56	15.53	14.45	14.80	11.35	11.17	16.94
0.39	1.70	1.35	1.40	1.27	1.26	1.26	1.76	1.70	2.92
1.88	3.85	3.55	4.20	5.00	4.60	4.20	0.77	0.88	1.53
0.02	0.09	0.09	0.06	0.06	0.06	0.09	0.02	0.01	0.07
0.23	1.24	0.87	0.91	2.56	1.12	1.57	0.21	0.42	3.06
0.48	3.34	2.36	3.35	3.29	3.58	1.69	0.84	0.32	4.89
4.12	3.91	4.39	3.52	3.61	3.73	3.71	2.08	1.71	3.52
4.52	3.06	3.20	3.84	1.97	3.19	3.00	6.17	5.11	1.41
0.04	0.15	0.11	0.14	0.12	0.14	0.11	0.02	0.04	0.09
0.09	0.04	0.07	0.07	0.91	0.09	0.13	0.11	0.07	0.25
0.94	0.81	1.02	0.97	2.50	0.94	1.87	0.47	1.00	1.80
99.79	99.80	99.85	99.82	99.82	99.82	99.36	99.74	99.77	99.78
0.91	1.28	1.37	0.92	1.83	1.17	1.24	0.34	0.33	2.50
0.16	0.29	0.25	0.23	0.43	0.26	0.34	0.14	0.24	0.57
5.80	15.3	16.2	17.5	18.9	17.7	16.7	5.67	5.64	11.3
10.8	45.9	26.1	50.1	113	50.9	65.7	30.3	12.9	85.0
24.7	30.3	42.9	76.6	36.9	25.9	40.4	23.7	26.9	44.5
1.77	8.51	5.41	6.38	14.9	7.30	8.21	2.48	2.23	12.6
8.07	64.7	18.0	34.7	7.30	6.96	12.4	8.13	8.92	33.6
19.9	19.3	19.2	20.4	20.0	21.7	19.4	14.3	15.3	16.4
74.5	85.2	91.8	128	67.4	111	91.7	178	149	32.7
49.1	207	219	242	155	248	247	164	63.7	453
48.0	36.9	37.0	39.6	28.9	40.0	35.7	41.6	41.9	12.1
279	326	333	344	301	354	411	260	238	110
9.76	11.5	10.9	11.9	9.37	12.3	11.3	7.49	7.15	4.68
623	461	494	559	359	482	422	1157	830	469
8.66	8.51	7.40	7.32	7.95	7.51	9.45	7.29	6.57	2.61
0.909	1.01	0.917	0.943	0.694	1.01	0.922	0.865	0.738	0.447
7.22	11.4	10.4	7.43	9.64	6.90	10.4	19.2	12.5	7.51
5.99	8.72	7.99	7.56	7.73	8.13	8.89	14.84	11.91	3.71
1.74	2.38	2.24	2.24	2.25	2.16	2.44	2.71	2.75	1.24
13.7	21.7	21.4	23.0	16.8	22.8	19.7	26.3	25.3	9.91
32.2	48.2	48.6	50.7	37.4	51.3	43.3	56.9	54.7	21.2
3.76	5.76	5.59	5.98	4.93	6.22	4.79	6.25	6.15	2.40
15.4	25.6	24.7	26.6	20.3	27.3	23.2	28.1	28.5	9.46
3.61	6.20	5.79	6.30	4.45	6.41	5.16	6.24	6.11	2.06
0.766	1.42	1.25	1.59	1.31	1.58	1.38	0.946	0.880	0.859
4.17	6.18	5.70	6.36	4.74	6.34	5.03	5.76	6.01	2.04
0.856	0.962	0.973	1.04	0.832	1.07	0.91	1.05	1.03	0.346
6.64	6.26	5.81	6.30	5.25	6.41	5.60	6.64	6.39	2.00
1.80	1.47	1.35	1.42	1.11	1.50	1.27	1.53	1.45	0.43
5.06	4.06	3.77	3.84	3.14	4.01	3.83	4.46	4.28	1.26
0.799	0.563	0.536	0.567	0.501	0.613	0.506	0.616	0.571	0.184
5.38	4.01	3.67	3.75	3.32	3.98	3.67	4.08	3.99	1.24
0.870	0.640	0.614	0.624	0.555	0.647	0.622	0.693	0.663	0.199

(*continued on next page*)

Table 2 (*continued*)

Sample	WXT740	WXT-740*	WXT-741	WXT742	WXT744	XT-28	XT-29	XT-27	XT-30	XT26
Longitude	81°46′128″	81°46′132″	81°46′135″	81°46′140″	81°46′323″	(a)	(a)	(a)	(a)	(a)
Latitude	45°14′002″	45°13′952″	45°13′948″	45°13′936″	45°13′810″	(a)	(a)	(a)	(a)	(a)
Rocks	Adakite	Adakite	Adakite	Adakite	Adakite	Adakite	Adakite	Adakite	Adakite	Adakite
SiO_2	62.31		62.05	62.33	74.42	61.90	72.36	62.39	63.64	61.23
TiO_2	0.56		0.57	0.59	0.31	0.60	0.32	0.66	0.50	0.69
Al_2O_3	16.60		16.76	16.73	12.64	16.71	13.60	17.37	17.40	18.25
Fe_2O_3	2.88		2.76	2.80	2.04	2.76	1.50	4.03	2.24	2.72
FeO	1.73		1.82	1.78	0.73	1.70	1.80	0.90	1.50	1.85
MnO	0.06		0.08	0.07	0.03	0.07	0.04	0.03	0.06	0.04
MgO	3.08		2.98	2.85	0.58	2.71	0.35	3.32	2.72	2.67
CaO	5.75		6.05	5.94	0.83	5.80	0.96	2.62	4.42	2.31
Na_2O	3.59		3.44	3.54	4.67	3.74	4.67	4.38	4.11	4.23
K_2O	1.41		1.57	1.50	2.83	1.58	3.07	1.32	1.34	1.78
P_2O_5	0.09		0.08	0.08	0.04	0.10	0.06	0.05	0.07	0.08
CO_2	0.04		0.04	0.04	0.04	0.05	0.02	0.05	0.07	0.79
H_2O	1.68		1.60	1.55	0.62	2.07	1.01	2.65	1.71	3.18
Σ	99.78		99.80	99.80	99.78	99.79	99.76	99.77	99.78	99.82
Na_2O/K_2O	2.55		2.19	2.36	1.65	2.37	1.52	3.32	3.07	2.38
$Mg^{\#}$	0.56		0.55	0.54	0.29	0.54	0.17	0.57	0.58	0.53
Sc	14.4	13.5	10.8	11.8	5.23	27.0	2.96	13.9	11.6	13.6
V	96.1	90.3	81.4	87.8	23.5	99.1	18.1	113	86.3	85.1
Cr	132	137	47.3	54.2	18.9	33.7	8.36	34.6	24.2	38.0
Co	16.1	15.5	13.9	15.0	3.15	14.4	3.43	14.3	12.5	12.7
Ni	98.8	95.2	31.2	26.5	2.84	20.4	4.25	20.2	18.6	21.3
Ga	18.1	17.8	16.0	16.6	5.80	17.1	11.3	17.7	17.6	17.5
Rb	29.8	29.6	36.3	37.4	63.0	43.3	68.6	36.8	38.9	56.6
Sr	499	500	421	432	284	493	486	432	540	379
Y	13.9	13.8	12.6	12.8	6.94	12.8	6.71	9.94	10.2	13.1
Zr	117	119	111	112	110	130	124	134	119	134
Nb	4.86	5.03	4.94	4.89	4.05	4.74	3.64	4.94	3.56	5.01
Ba	510	508	395	411	854	463	863	618	550	347
Hf	2.83	2.67	2.51	2.86	2.66	3.70	3.20	3.59	3.12	3.49
Ta	0.452	0.458	0.463	0.459	0.416	0.666	0.382	0.518	0.378	0.492
Pb	7.31	7.29	7.00	7.64	4.35	7.79	5.63	6.85	8.96	4.97
Th	4.11	3.87	3.11	3.77	3.27	4.01	3.88	4.11	3.37	3.84
U	1.18	1.17	1.02	1.29	0.847	1.28	1.03	1.21	1.10	0.875
La	11.4	11.6	10.3	10.5	10.1	11.3	11.8	7.89	10.1	8.44
Ce	24.0	25.1	22.2	21.7	18.9	23.3	20.7	16.6	20.6	22.4
Pr	2.72	2.85	2.61	2.52	1.84	2.96	2.21	2.05	2.51	2.90
Nd	11.4	11.5	10.3	11.1	7.13	11.7	7.96	8.08	9.89	11.8
Sm	2.46	2.49	2.34	2.31	1.27	2.49	1.38	1.71	1.99	2.31
Eu	0.900	0.927	0.842	0.877	0.658	0.849	0.388	0.776	0.734	0.741
Gd	2.58	2.56	2.55	2.16	1.17	2.36	1.12	1.83	1.97	2.24
Tb	0.394	0.390	0.364	0.372	0.194	0.406	0.186	0.316	0.329	0.387
Dy	2.24	2.31	2.05	2.17	1.14	2.38	1.19	1.94	1.91	2.36
Ho	0.48	0.472	0.431	0.450	0.220	0.485	0.237	0.394	0.375	0.474
Er	1.41	1.36	1.26	1.40	0.740	1.34	0.710	1.158	1.08	1.35
Tm	0.180	0.191	0.181	0.192	0.097	0.214	0.111	0.184	0.171	0.209
Yb	1.29	1.28	1.24	1.32	0.739	1.39	0.798	1.27	1.10	1.37
Lu	0.227	0.223	0.203	0.215	0.13	0.24	0.142	0.214	0.181	0.241

(biotite) flux monitors, and irradiated for 37 h at Beijing Nuclear Research Center. The monitor samples were individually fused and analyzed for argon-isotope compositions. All samples were step-heated using a radio-frequency furnace. Argon isotope analyses were conducted on a MM-1200 mass spectrometer at the Laboratory of analyzing center, Guilin Resource and Geological Institute. The monitor standard was the ZBH-25 (biotite, 132.5 Ma) and ages were calculated using the constants recommend by Steiger and Jäger (1977). All errors are quoted at the 1σ level and do not include the uncertainly of the monitor age. The experimental procedures were described in details by Dai and Hong (1982) and Wang et al. (2003).

Relatively fresh samples (e.g., most andesites, dacites and rhyolites) chosen for elemental and isotopic analysis were first split into small chips and ultrasonically cleaned in distilled water and dried, and then powdered. Some samples (e.g., basalts and basaltic andesites and a small proportion of andesites and dacites) with pores or slight alteration were first split into small chips and soaked in 4N hydrochloric acid for 1 h to remove secondary carbonate minerals, then powdered after rinsing with distilled water and drying. Major elements were determined at the Hubei Institute of Geology and Mineral Resources, by X-ray fluorescence spectrometry with analytical errors less than 2%. The FeO contents of the samples were analyzed by a conventional wet chemical titration method described in detail by Gao et al. (1995) and Wu et al. (2002). Trace elements, including the rare earth element (REE), were analyzed by a Perkin-Elmer ELAN 6000 inductively-coupled plasma source mass spectrometer (ICP-MS) at the Guangzhou Institute of Geochemistry, Chinese Academy of Sciences following procedures described by Li et al. (2002b), and China University of Geosciences (Wuhan) following procedures described by Hu et al. (2000b) and Wu et al. (2002), respectively. At Guangzhou, the powdered samples (50 mg) were dissolved in screw-top Teflon beakers using an HF+HNO_3 mixture for 7 days at ~100 °C. An internal standard solution containing the single element Rh was used to monitor drift in mass response during counting. USGS standard BCR-1 was used to calibrate the elemental concentrations of the measured samples. Analytical precision for most elements was better than 3% (Li et al., 2002b). In Wuhan, samples were dissolved in a two-step procedure to ensure refractory mineral dissolution. First, a mixture of HF+HNO_3 was added to each sample in a capped Teflon beaker and the beaker was placed on hot plate for evaporation. The solution was then dried, re-dissolved in HF+HNO_3, and the entire solution-residue assemblage was transferred into Teflon bombs with HCl+HF+HNO_3. The bomb dissolution lasted for 4 days at a temperature of ~140–190 °C. By then, no residue was detectable. The solutions were then transferred back into Teflon beakers and evaporated on a hot plate. The final precipitate was dissolved in dilute HNO_3 for ICP-MS analysis; the analytical precision for most elements is greater than 10% (Hu et al., 2000b; Wu et al., 2002).

The Sr and Nd isotopic compositions were determined using a Finnigan MAT-262 Mass Spectrometer at the Institute of Geology and Geophysics, Chinese Academy of Sciences, using essentially the same procedures as Zhang et al. (2002). The $^{87}Sr/^{86}Sr$ ratio of the NBS987 standard and $^{143}Nd/^{144}Nd$ ratio of the La Jolla standard measured during this study are 0.710246±9 (2 σm) and 0.511854±8 (2σ m), respectively. Overall blank contributions are about 0.2–0.5 ng for Rb and Sr, and about 50 pg for Nd and Sm. The Rb, Sr, Sm, and Nd concentrations exhibit good agreement with those analyzed using ICP-MS. The measured $^{143}Nd/^{144}Nd$ and $^{86}Sr/^{88}Sr$ ratios are normalized to $^{146}Nd/^{144}Nd=0.7219$ and $^{86}Sr/^{88}Sr=0.1194$, respectively.

4. Results

$^{40}Ar/^{39}Ar$ geochronology, major and trace element, and Nd–Sr isotope data of the Alataw volcanic rocks are listed in Tables 1, 2 and 3, respectively. As described below, the data, establish that volcanic rocks in the Alataw area can be classified as Early Carboniferous adakites and NEBs and Late Carboniferous calk-alkaline to high-K calk-alkaline andesites, dacites and rhyolites.

4.1. Geochronology

^{40}Ar–^{39}Ar age spectra for the adakite, NEB and non-adakitic dacite in the Alataw area are plotted in Fig. 3. Three samples WXT740 (adakite), WXT721 (NEB) and WXT733 (non-adakitic dacite) yielded plateau ages of 320±1 Ma, 319±2 Ma and 306±4 Ma, respectively. The latter age is consistent with the data of Chen et al. (1994, 2000b), who published ages of ca. 310 Ma for the high-K andesites and rhyolites, 307 Ma for compositionally equivalent I-type granitoids, and ca. 290 Ma for S-type granitoids in the Alataw area. In the context of the northern Tianshan Range, the Alataw data establish a record of relatively continuous magmatism extending from the ~325 Ma formation age of the Bayinggou ophiolite through to granite emplacement, all of which significantly predate intrusion of the possibly plume-related Huangshan mafic-ultramafic suite at 269±2 Ma (Zhou et al., 2004).

Table 3
Sr–Nd isotopic compositions of Carboniferous volcanic rocks in the Alataw area

Sample	Rocks	Sm (ppm)	Nd (ppm)	$^{147}Sm/^{144}Nd$	$^{143}Nd/^{144}Nd$	$2s_m$	t(Ma)	$f_{Sm/Nd}$	$(^{143}Nd/^{144}Nd)_i$	ε_{ND} (t)	T_{DM} (Ga)	Rb (ppm)	Sr (ppm)	$^{87}Rb/^{86}Sr$	$^{87}Sr/^{86}Sr$	$2s_m$	$(^{87}Sr/^{86}Sr)_i$	References
P201	NEB	5.07	26.45	0.1159	0.513062	±7	320	−0.41	0.512819	11.6	0.14	5.24	388.5	0.039	0.70427	±2	0.7041	(a)
P154-3	NEB	7.20	28.97	0.1503	0.512897	±6	320	−0.24	0.512582	7.0	0.61	9.81	335.0	0.080	0.70107	±4	0.7007	(a)
XT-17	NEB	8.057	30.50	0.1598	0.512889	±7	320	−0.19	0.512554	6.4	0.74	4.00	354.0	0.1708	0.705518	±24	0.7047	(b)
WXT721	NEB	5.808	20.66	0.1710	0.512996	±12	320	−0.13	0.512638	8.0	0.55	18.22	905.0	0.05824	0.706584	±11	0.7063	(b)
XT-27	Adakite	1.709	8.077	0.1287	0.512832	±14	320	−0.35	0.512562	6.6	0.57	36.80	431.6	0.2466	0.704643	±9	0.7035	(b)
XT-28	Adakite	2.722	12.43	0.1325	0.512678	±6	320	−0.33	0.512400	3.4	0.89	43.28	493.4	0.2453	0.704918	±23	0.7038	(b)
XT-29	Adakite	1.377	7.956	0.1053	0.512753	±13	320	−0.46	0.512532	6.0	0.56	68.63	486.2	0.4083	0.705729	±11	0.7039	(b)
XT-30	Adakite	1.803	8.270	0.1320	0.512751	±10	320	−0.33	0.512474	4.8	0.74	36.03	509.2	0.2048	0.705092	±19	0.7042	(b)
WXT742	Adakite	2.451	11.15	0.1331	0.512774	±14	320	−0.32	0.512495	5.3	0.71	37.06	409.8	0.2596	0.704762	±16	0.7036	(b)
WXT734	Dacite	6.105	25.88	0.1428	0.512639	±10	306	−0.27	0.512340	2.2	1.10	104.30	242.2	1.234	0.710395	±13	0.7048	(b)
WXT737	Rhyolite	1.201	3.22	0.2260	0.513027	±20	306	0.15	0.512554	6.4		79.45	86.07	2.653	0.717056	±17	0.7050	(b)
P152	Andesite	5.40	22.14	0.1475	0.512656	±11	306	−0.25	0.512347	2.4	1.14	64.35	206.8	0.900	0.70779	±6	0.7037	(a)
P93-1	Rhyolite	7.44	33.06	0.1361	0.512572	±6	306	−0.31	0.512287	1.2	1.13	158.5	161.1	2.85	0.71890	±7	0.7059	(a)
P175	Rhyolite	8.86	36.24	0.1779	0.512658	±8	306	−0.10	0.512285	1.2	2.09	151.2	57.15	7.68	0.73675	±6	0.7018	(a)
P203	Rhyolite	10.56	40.46	0.1578	0.512839	±6	306	−0.20	0.512508	5.5	0.85	119.2	69.25	4.99	0.72594	±6	0.7032	(a)
Bb-45	Basalt (OPh)			0.2112	0.512949	±18	320	0.07	0.512507	5.47				0.133	0.707404	±15	0.7068	(c)
Bb-57	Basalt (OPh)			0.2015	0.512856	±11	320	0.02	0.512434	4.06				0.050	0.705056	±16	0.7048	(c)
Bb-58	Basalt (OPh)			0.2055	0.512920	±10	320	0.04	0.512489	5.14				0.100	0.704848	±18	0.7044	(c)
Bb-62	Basalt (OPh)			0.1932	0.513070	±9	320	−0.02	0.512665	8.57				0.139	0.705669	±15	0.7050	(c)
Bb-71	Basalt (OPh)			0.2075	0.512927	±15	320	0.05	0.512492	5.20				0.094	0.705476	±16	0.7050	(c)
Bb-73	Basalt (OPh)			0.2346	0.513161	±16	320	0.19	0.512670	8.66				0.163	0.706060	±19	0.7053	(c)
Bb-78	Basalt (OPh)			0.2195	0.513225	±13	320	0.12	0.512765	10.52				0.886	0.707160	±20	0.7031	(c)
Bb-79	Basalt (OPh)			0.2058	0.512913	±15	320	0.05	0.512482	4.99				0.467	0.705799	±17	0.7037	(c)
Bb-10	Basalt (OPh)			0.2070	0.512898	±12	320	0.05	0.512464	4.65				0.425	0.706250	±19	0.7043	(c)
BT4	Basalt (OPh)			0.1955	0.512794	±10	320	−0.01	0.512384	3.09				0.400	0.705569	±19	0.7037	(c)

(a) Chen et al. (2000b); (b) this study; (c) Xu et al. (2006) and references therein. NEB: Nb-enriched basalts and basaltic andesites; Oph: ophiolite in the Bayingou area. $f_{Sm/Nd}=[(^{147}Sm/^{144}Nd)_{sample}/(^{147}Sm/^{144}Nd)_{CHUR}]-1$, $TDM=1/\lambda_{Sm}\ln\{[(^{143}Nd/^{144}Nd)_{sample}-(^{143}Nd/^{144}Nd)_{DM}]/[(^{147}Sm/^{144}Nd)_{sample}-(^{147}Sm/^{144}Nd)_{DM}]\}$, $(^{147}Sm/^{144}Nd)_{CHUR}=0.1967$, $(^{143}Nd/^{144}Nd)_{DM}=0.51315$, $(^{147}Sm/^{144}Nd)_{DM}=0.2137$, $\lambda_{Sm}=0.00654\ Ga^{-1}$.

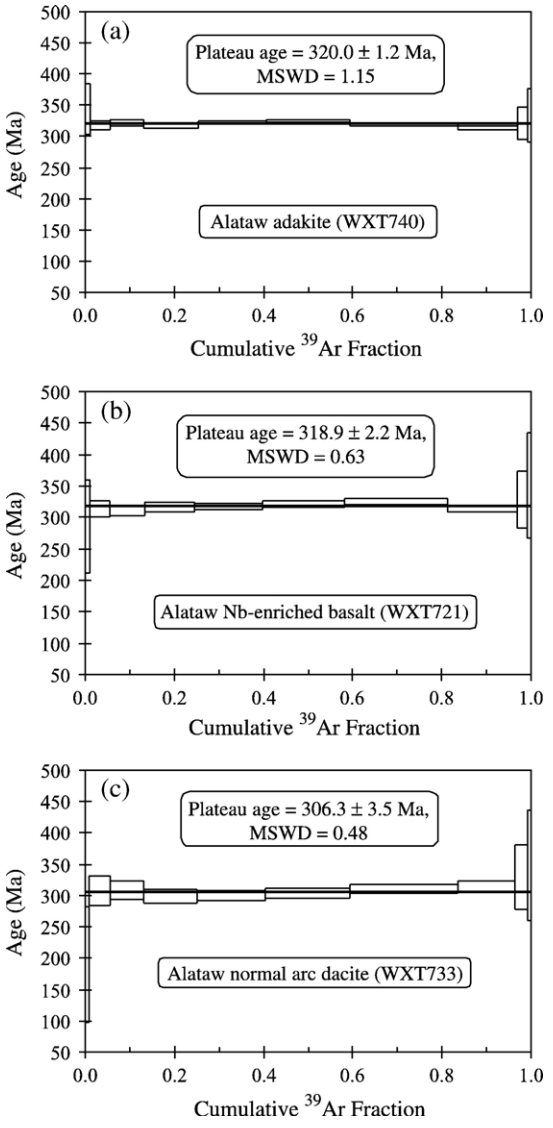

Fig. 3. The $^{40}Ar/^{39}Ar$ age spectra diagrams for adakite, NEB and normal arc dacite.

4.2. Petrological and geochemical characteristics

4.2.1. Non-adakitic ("high-K") andesites, dacites and rhyolites

Late Carboniferous andesites, dacites and rhyolites constitute distinct sequences in the Alataw Mountains (Fig. 4). These rocks typically contain varying proportions of plagioclase, potassium feldspar, quartz, magnetite and minor hornblende and biotite phenocrysts in cryptocrystalline-glassy matrices. Like the I-type granitoids in the Alataw area, they are mainly high-K calc-alkaline (Fig. 5a). For convenience, they are collectively referred to here as the "high-K suite". In the major- and trace-element Harker diagrams (Figs. 5 and 6), K_2O and strongly incompatible elements (e.g., Th and Rb) of the high-K suite, I-type granitoids, and NEBs all exhibit positive correlations, whereas Al_2O_3, CaO, MgO, FeO_{total} ($FeO+Fe_2O_3\times0.9$), P_2O_5, strongly compatible elements (e.g., Co and Cr), intermediately incompatible element Sr and incompatible element Zr display negative correlations or lack significant correlations. The most obvious characteristic of the Alataw high-K suite is its similarity to common arc andesites, dacites and rhyolites, e.g., enrichment of light rare earth elements (LREE; Fig. 7a), high heavy REE (HREE) (e.g., Yb=2.99–7.10 ppm) and Y (29–65 ppm) contents, distinctly negative anomalies of Eu, Nb, Sr and Ti (Fig. 7a and b, and Table 2), and low Sr contents (49–248 ppm) and Sr/Y ratios (1–7) (Table 2 and Fig. 8). The coeval I-type granitoids exhibit similar geochemical characteristics (Figs. 7a and b and 8).

4.2.2. NEBs

The NEBs mainly occur in the western Aibi Lake, Alataw areas. They consist of arc basalts and basaltic andesites (Fig. 4) that contain phenocrysts (plagioclase and augite), matrices (magnetite, titanomagnetite and cryptocrystalline-glassy material), and minor secondary carbonates filling in pores. None of these basaltic rocks are nepheline normative, and all plot within the subalkaline field (Fig. 4). They are sodium-rich (Na_2O/K_2O=2.03–8.06) and plot in the low- and medium-K calc-alkaline field (Fig. 5a). Their chondrite normalized REE patterns are not strongly fractionated and they lack Eu anomalies (Fig. 7c). They are distinguished from typical arc basalts by their higher Zr (209–356 ppm), TiO_2 (2.00–3.56 wt.%), P_2O_5 (0.29–0.57 wt.%) and Nb (5.87–12.9 ppm) contents and higher $(Nb/Th)_{PM}$ (0.51–3.13), $(Nb/La)_{PM}$ (0.57–1.29),

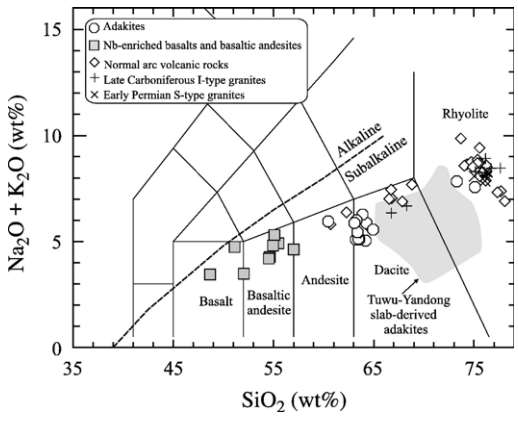

Fig. 4. K_2O+Na_2O versus SiO_2 (classification from Le Bas et al. (1986)). The borderline between alkaline and subalkaline volcanic rocks is after Irvine (1971). Data sources for the igneous rocks in the Alataw area are from Chen et al. (2000b) and this study. Data sources for the Tuwu–Yandong adakites are from Xiong et al. (2005) and Zhang et al. (2006).

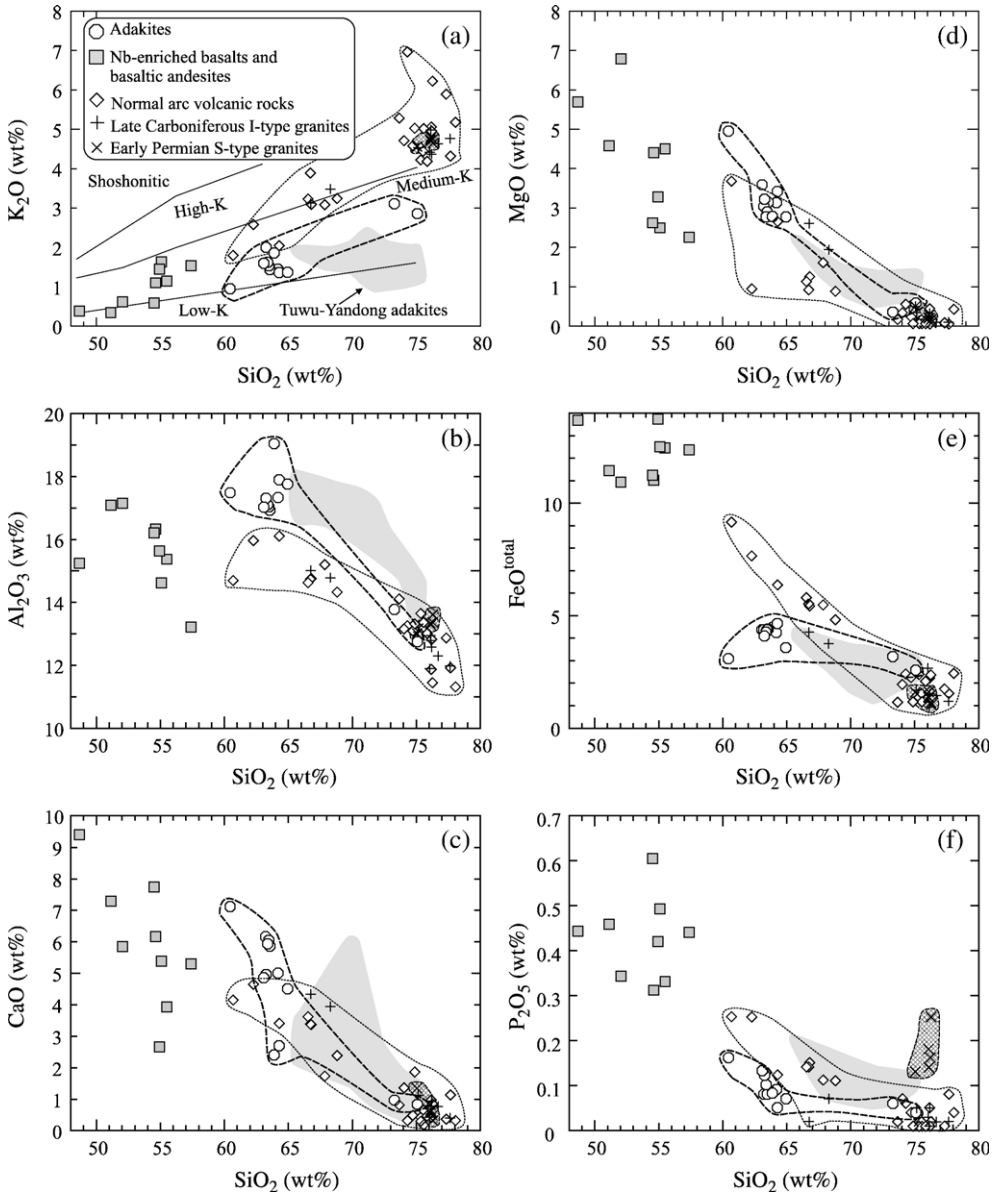

Fig. 5. Harker diagrams showing the major element variations of the igneous rocks in the Alataw area. Original K_2O versus SiO_2 (wt.%) classification diagram (a) is after Peccerillo and Taylor (1976). Data sources for the igneous rocks in the Alataw area and the Tuwu–Yandong adakites are the same as in Fig. 4.

Nb/U (15–26) ratios (Table 2 and Fig. 9). They are different from OIB, N-MORB and E-MORB (Sun and McDonough, 1989) in that they have lower Nb/U and Ce/Pb (4.72–15.81) ratios (Fig. 9c and Table 2) and occasional positive anomalies in Ba, Sr and Zr (Fig. 7d). However, they exhibit incompatible element-enriched normalized patterns with minor negative or positive anomalies in Ba, Nb, Sr, Zr and Ti (Fig. 7d), which are almost identical to those of the Philippines and Mexico NEBs (e.g., Sajona et al., 1993, 1996; Aguillón-Robles et al., 2001).

4.2.3. Adakites

Adakites in the Alataw Mountains occur mainly in the Halatulukegou area (Fig. 2) and consist of andesites, dacites and rhyolites (Fig. 4). Rhyolitic adakites (cf., Defant and Drummond, 1990) contain phenocrysts of plagioclase, quartz, magnetite and minor potassium feldspar, hornblende and biotite. Andesitic and dacitic adakites contain phenocrysts of plagioclase, augite, magnetite, hornblende, and minor biotite and microcrystals of plagioclase and augite in the matrix. The Alataw adakites are calc-alkaline

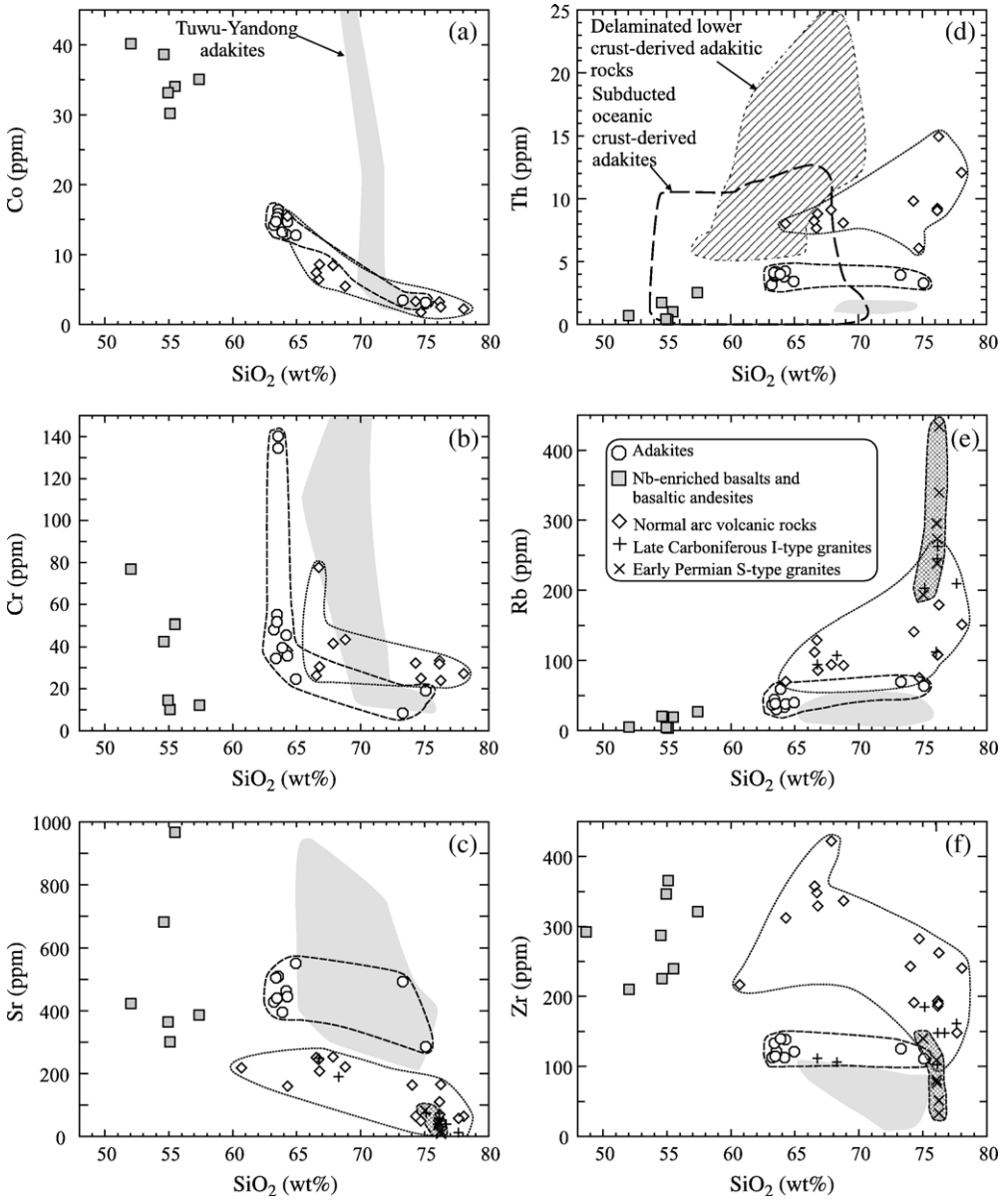

Fig. 6. Harker diagrams showing the trace element variations of the igneous rocks in the Alataw area. Data sources for the igneous rocks in the Alataw area and the Tuwu–Yandong adakites are the same as in Fig. 4. The field of subducting oceanic crust-derived adakites is constructed using data from the following sources: Defant and Drummond, 1990; Kay et al., 1993; Stern and Kilian, 1996; Sajona et al., 1993; Aguillón-Robles et al., 2001; Defant et al., 2002; Martin et al., 2005, and references therein. Data source for delaminated lower crust-derived adakitic rocks are after Wang et al. (2006, and references therein).

in composition (Table 2 and Fig. 5a). Like typical adakites the world over (e.g., Defant and Drummond, 1990, 1993; Kay et al., 1993) or Early Carboniferous adakites in the Tuwu–Yangdong area, northern Tianshan Range (Xiong et al., 2005; Zhang et al., 2006), they are characterized by high Na_2O/K_2O (1.52–3.32) ratios, fractionated REE patterns with slight concavities of middle REE, negligible to positive Eu anomalies (Fig. 7e), strong depletion of HREE (e.g., Yb = 0.74–1.47 ppm) and Y (6.7–14.9 ppm), and positive Sr and Ba but negative Nb and Ti anomalies (Table 2, Fig. 7f). They all plot in the field of adakites on a Sr/Y versus Y diagram (Fig. 8) and in the fields of "high-silica andesite" recently defined by Martin et al. (2005; Fig. 10). The rhyolitic Alataw adakites differ from the andesitic and dacitic examples in that the former has lower Al_2O_3, CaO, MgO and compatible elements (e.g., Co, Cr) contents than the latter (Figs. 5b–d and 6a–b, Table 2). However, all of the adakites have similar incompatible

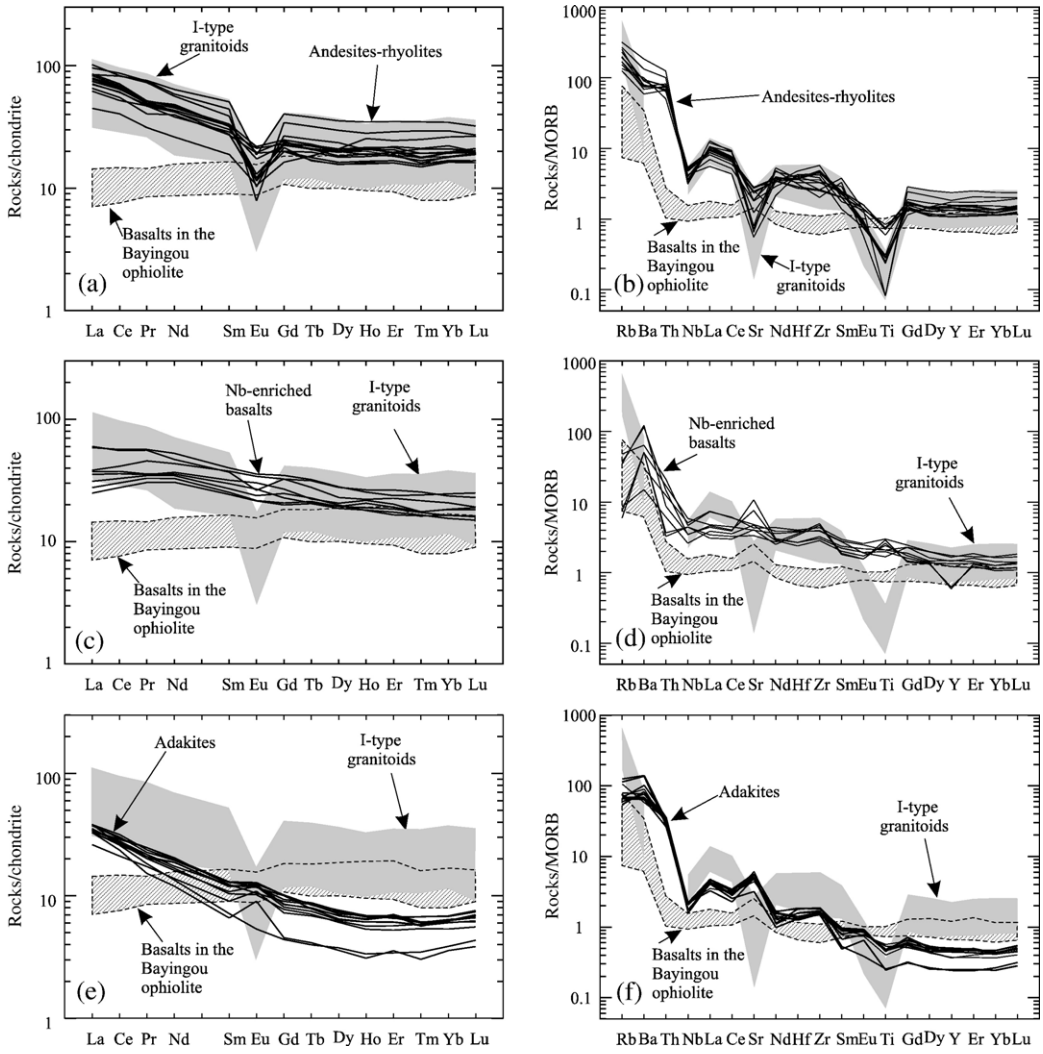

Fig. 7. Primitive mantle-normalized rare earth element (REE) patterns (a, c and e) and N-MORB-normalized muti-elements profiles (b, d and f) for igneous rocks in the Alataw area. N-MORB normalizing values are from Sun and McDonough (1989); chondrite normalizing values are from Boynton (1984). Data sources for the igneous rocks in the Alataw area are the same as in Fig. 4. Data sources for basalts from the Bayingou ophiolites from Xu et al. (2006 and references therein).

element contents (e.g., Th, Rb and Zr; Fig. 6d–f). Collectively, the adakites define major- and trace-element compositional trends that are distinct from those of the Alataw high-K volcanic suite, I-type granitoids, and NEBs (Figs. 5 and 6).

4.3. Nd–Sr isotope geochemistry

The Nd–Sr isotope compositions of Carboniferous–Early Permian magmatic rocks and Proterozoic gneisses and amphibolites of the basement in the Alataw area are shown in Fig. 11. All magmatic rocks have positive $\varepsilon_{Nd}(T)$ values between +0.1 and +11.6. Four NEB samples include the highest $\varepsilon_{Nd}(T)$ values ranging from +6.4 to +11.6, but overlap other Alataw suites in terms of $(^{87}Sr/^{86}Sr)_i$ ratios, which range between 0.7007 and 0.7063 (Table 3, Fig. 11). Six samples of the high-K suite display $\varepsilon_{Nd}(T)$ values ranging from +1.2 to +6.4 and $(^{87}Sr/^{86}Sr)_i$ ratios varying between 0.7018 and 0.7059, which are similar to those of the Alataw I-type granitoids (Table 3, Fig. 11). Five adakite samples exhibit relatively constant $\varepsilon_{Nd}(T)$ values (+3.4–+6.6) and $(^{87}Sr/^{86}Sr)_i$ ratios (0.7035–0.7042), which overlap those of MORB, Cenozoic slab-derived adakites, the Tuwu–Yandong adakites, and basalts from the Early Carboniferous Ophiolites in the Bayingou area (Table 3, Fig. 11). The positive $\varepsilon_{Nd}(T)$ values of Early Permian S-type granitoids (Fig. 11; Chen et al., 2000b) distinguish them from typical S-type

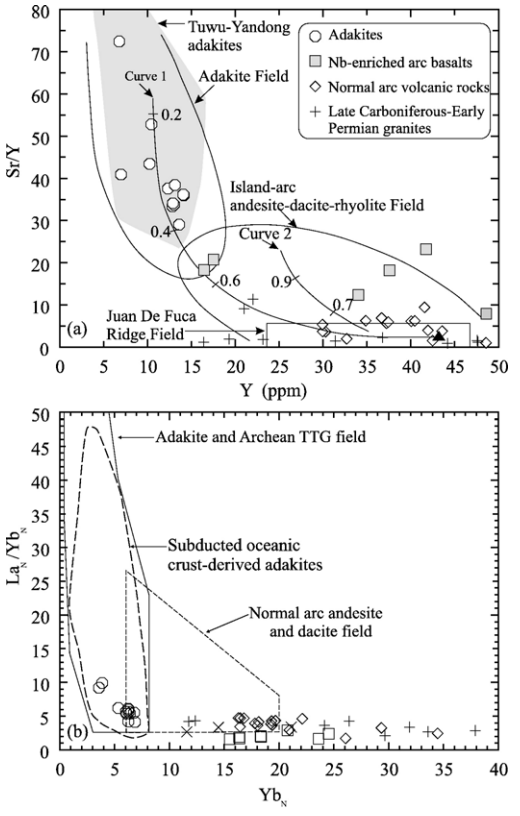

Fig. 8. (A) Sr/Y versus Y diagram (Defant and Drummond, 1993). Juan de Fuca basalt field and Curve 1 and 2 are from Defant and Drummond (1993). Sample O16-6 (Y=44.6 ppm; Sr=159 ppm) was used for partial melting model (Curve 1). Residual minerals: 35% clinopyroxene, 30% amphibole, and 35% garnet. Various F values (amount of melt) are plotted along the Curve 1. Sample 52 (Y=25 ppm; Sr=576 ppm) was used for crystal fractionation model (Curve 2). Fractionating phase: 30% clinopyroxene, 30% orthopyroxene, and 40% plagioclase. Various F values (amount of remaining melt) are plotted along the Curve 2. Modelling results are from Defant and Drummond (1993). Data sources for the igneous rocks in the Alataw area and the Tuwu–Yandong adakites are the same as in Fig. 4. (B) La_N/Yb_N versus Yb_N diagram (Martin, 1999). The field for subducted oceanic crust-derived adakites are after Wang et al. (2006).

granites (McCulloch and Chappell, 1982). However, they do exhibit high $(^{87}Sr/^{86}Sr)_i$ ratios (0.7081–0.7148) similar to typical S-type granites (McCulloch and Chappell, 1982) (Fig. 11). As a whole, the high-K suite and I- and S-type granitoid samples display relatively low $\varepsilon_{Nd}(T)$ values (Fig. 11b) compared to those of adakites and NEBs.

5. Discussion

5.1. Petrogenesis of adakites

Defant and Drummond (1990) initially characterised adakites as andesitic to rhyolitic Na-rich igneous rocks formed in modern arcs where young and hot lithosphere was being subducted. They noted that the trace element compositions of these magmas are consistent with derivation from partial melting of subducting oceanic crust under eclogite facies or garnet bearing amphibolite conditions. This model is supported by a number of

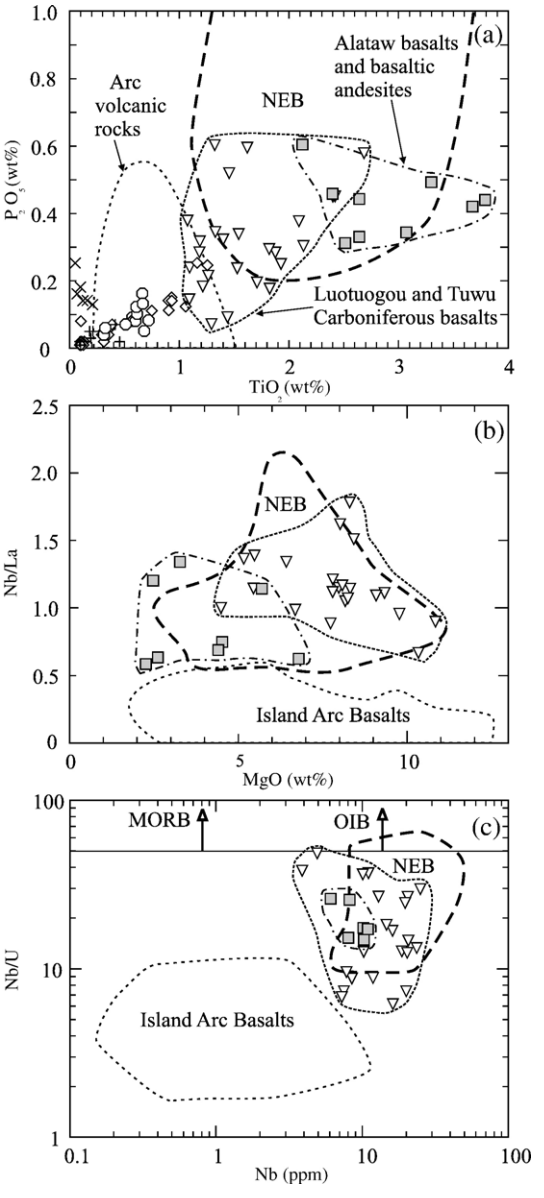

Fig. 9. (a) P_2O_5 versus TiO_2 diagram. The fields of the arc volcanic rocks and Nb-enriched (or High-Nb) arc basalts (NEB) are from Defant et al. (1992). (b) Nb/La versus MgO (wt.%) diagram (Kepezhinskas et al., 1996). (c) Nb/U versus Nb diagram (Kepezhinskas et al., 1996). The fields of the island arc basalts and NEB are from Kepezhinskas et al. (1996). The field of the Luotuogou and Tuwu Carboniferous basalts is constructed using data from the following sources: Xia et al., 2004b; unpublished data of Q. Wang. Data sources for the igneous rocks in the Alataw area are the same as in Fig. 4.

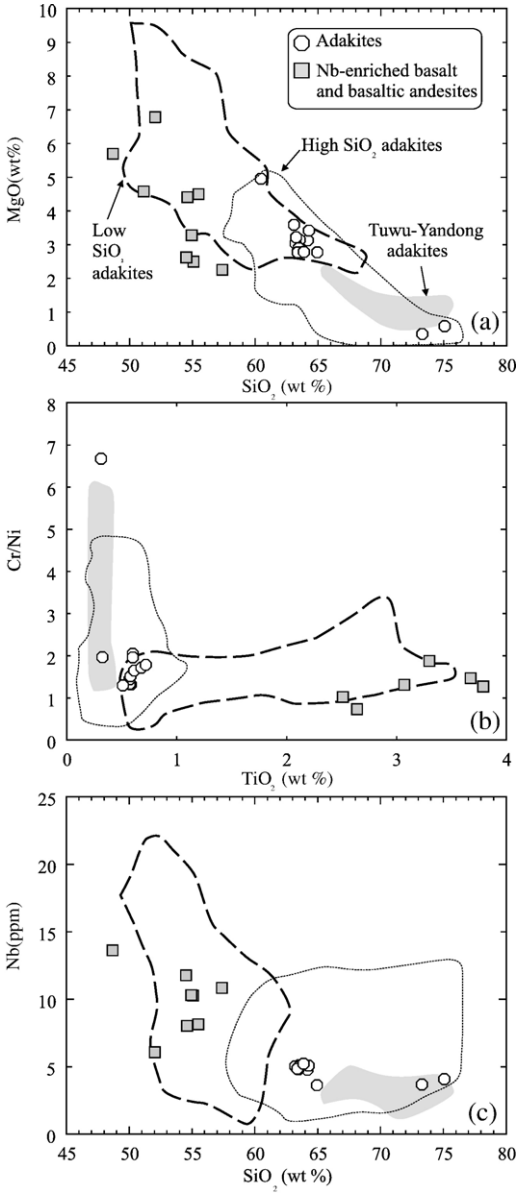

Fig. 10. Variation diagrams comparing the fields of high- and low-silica adakites, as defined by Martin et al. (2005), and the Alataw adakites and NEBs. (a) MgO versus SiO_2. (b) Cr/Ni versus TiO_2. (c) Nb versus SiO_2. Data sources for the igneous rocks in the Alataw area and the Tuwu–Yandong adakites are the same as in Fig. 4.

studies of Cenozoic adakites (e.g., Kay et al., 1993; Yogodzinski et al., 1995; Stern and Kilian, 1996). However, several other mechanisms have also been proposed to account for the origin of specific occurrences of adakites and adakitic rocks. These include: (1) generation of "low-silica adakites" (or magnesian andesites) via partial melting of slab-melt modified mantle wedge (Martin et al., 2005); (2) crustal assimilation and fractional crystallization (AFC) processes from parental basaltic magmas (e.g., Castillo et al., 1999); (3) partial melting of hydrated mafic rocks in the lower part of a thickened crust (e.g., Atherton and Petford, 1993; Petford and Atherton, 1996; Zhang et al., 2001; Xiong et al., 2003; Chung et al., 2003; Condie, 2005; Wang et al., 2005); (4) partial melting of delaminated lower crust (e.g., Kay and Kay, 1993; Xu et al., 2002; Gao et al., 2004; Wang et al., 2004a,b, 2006).

Geochemical evidence precludes generation of the Alataw adakites by fractionation of coeval basaltic magmas. The adakites do not exhibit fractional crystallization trends with the NEBs on Harker diagrams (Figs. 5 and 6), given their high Al_2O_3, Cr and Sr contents, approximately constant Th, Rb and Zr

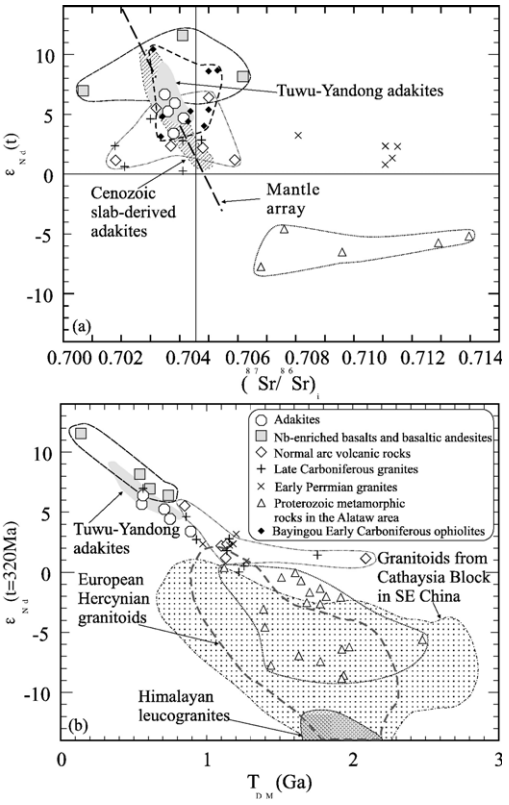

Fig. 11. Nd–Sr isotope (a) and $\varepsilon_{Nd}(t=320\ Ma)$ versus T_{DM}(Ga) (b) diagrams for the igneous rocks and Proterozoic metamorphic rocks in the Alataw area. Cenozoic subducting oceanic crust-derived adakites are after Defant et al. (1992), Kay et al. (1993), Stern and Kilian (1996) and Aguillón-Robles et al. (2001). The fields for the granitoids from European, Cathaysia Block in SE China and Himalayan are after Jahn et al. (2000a), and references therein. Data for Proterozoic metamorphic rocks in the Alataw area are after Chen et al. (2000b) and Hu et al. (2000a). Data sources for the igneous rocks in the Alataw area and the Tuwu–Yandong adakites are the same as in Fig. 4. Data sources for basalts from the Bayingou ophiolites from Xu et al. (2006 and references therein).

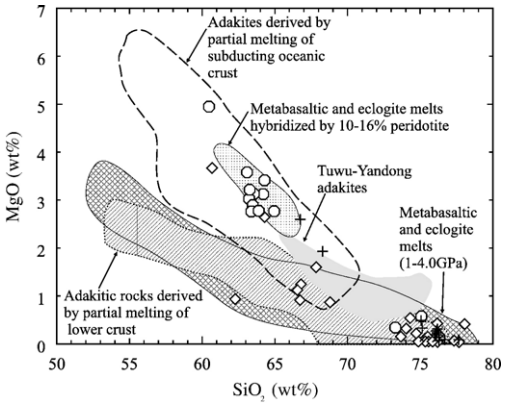

Fig. 12. MgO versus SiO_2 (wt.%) diagram for the igneous rocks in the Alataw area. The field of subducting oceanic crust-derived adakites is constructed using data from the following sources: Defant and Drummond, 1990; Kay et al., 1993; Sajona et al., 1993; Stern and Kilian, 1996; Aguillón-Robles et al., 2001; Defant et al., 2002; Martin et al., 2005, and references therein. The data of metabasaltic and eclogite experimental melts (1–4.0 GPa) are from the following: Rapp et al., 1991; Sen and Dunn, 1994; Rapp and Watson, 1995; Winther, 1996; Springer and Seck, 1997; Rapp et al., 1999, 2002; Skjerlie and Patiño Douce, 2002, and references therein. The data of metabasaltic and eclogite experimental melts hybridized by peridotite are after Rapp et al. (1999). The data of adakitic rocks derived by partial melting of lower crust are from Atherton and Petford (1993), Muir et al. (1995), Petford and Atherton (1996) and Johnson et al. (1997). Data sources for the igneous rocks in the Alataw area and the Tuwu–Yandong adakites are the same as in Fig. 4.

contents, and their relatively low light REE contents compared to coeval basalts (Fig. 7c and e).

Partial melting of the lower crustal is not supported by the high MgO contents (Fig. 12) of the andesitic adakites compared to either natural adakitic rocks derived from thick lower crust-derived or experimental melts of metabasaltic and eclogite melts (1–4.0 GPa). Their much higher $\varepsilon_{Nd}(T)$ values and lower $(^{87}Sr/^{86}Sr)_i$ ratios compared to Proterozoic metamorphic rocks in the Alataw area also preclude adakite formation by partial melting of old metamorphic rocks.

Partial melting of delaminated or foundering lower crust resembles slab melting in many respects (Kay and Kay, 2002). Although this origin cannot be entirely ruled out, recognised examples of adakites generated by this process have relatively high K contents (~3 wt.% K_2O), are distinctly enriched in Th (10–20 ppm), probably due to the greater involvement of highly evolved felsic crustal material, and are associated with evidence of contemporaneous crustal thinning (eg., Wang et al., 2004a, 2006). Plank (2005) considered that lower-crustal delamination provides an ideal mechanism to both generate high-Th or Th/La melts and remove low-Th or Th/La cumulates and restites from the continental crust. The absence of high Th contents in the Alataw adakites suggest they were unlikely to have been derived by the melting of delaminated lower crust.

Many modern adakites are associated with the subduction of young, hot oceanic slabs such as in the western Aleutian Island (Yogodzinski et al., 1995); Philippines (Sajona et al., 1993, 1996), Central America (Defant et al., 1992) and South America (Stern and Kilian, 1996; Sigmarsson et al., 1998). Several lines of evidence suggest that the Alataw adakites were generated by this mechanism. Tectonic studies indicate that a Carboniferous ocean closed in the northern Tianshan area, and that oceanic crust subducted southwestward beneath the Yili–middle-Tianshan Plate, resulting in a Carboniferous island arc at the northeastern margin of the Yili–middle-Tianshan Plate (Windley et al., 1990; Xiao et al., 1992; Hsü et al., 1994; Li et al., 2002a; Qin et al., 2002; Zhao et al., 2003; Zhou et al., 2004; Liu and Fei, 2006). In particular, the early Carboniferous (325±7 Ma) age of the Bayinggou ophiolites in the Northern Tianshan Variscan fold belt (Xu et al., 2006) overlaps the 320±1 Ma age determined for the Alataw adakites. Given that many ophiolites form in the earliest stages of arc development (Bloomer et al., 1995), the Bayinggou examples probably developed in response to the opening of the Carboniferous ocean in the northern Tianshan (eg., Huang et al., 1990) and therefore signify a strong potential for the presence of young oceanic crust. Moreover, the Alataw adakites have Nd–Sr isotope compositions similar to the basalts from the approximately coeval ophiolite in the Bayingou area (Xu et al., 2006) and slab-derived adakites in the Tuwu–Yandong area (Fig. 11) (Xiong et al., 2005; Zhang et al., 2006), strongly supporting an origin linked to partial melting of subducted oceanic crust. Additionally, the Alataw adakites are similar to adakites from modern arcs (Defant and Drummond, 1990; Kelemen et al., 2003; Plank, 2005) and the Tuwu–Yandong adakites (Zhang et al., 2006) in that they have relatively low K_2O and Th contents (Figs. 5a and 6d), indicating that they mainly originate from the basaltic portion of subducting slabs without a major sedimentary component (e.g., Plank, 2005). A similar argument must then be applicable to the relatively low La contents of the Alataw adakites (~10 ppm: Table 2). Other adakites occurrences with similarly low La abundances, include Pichincha, Ecuador (10.8–11.5 ppm La: Bourdon et al., 2003), Zamboanga, Philippines (10.8–11.5 ppm La: Sajona et al., 1993), and Kamchatka (6–14.8 ppm La: Kepezhinskas et al., 1996).

The strong depletion of HREE and Y contents, and positive Sr and negligible to positive Eu anomalies of the Alataw adakite imply that partial melting of source rocks took place in the garnet stability field, and that garnet, rather than plagioclase, was left as a residual

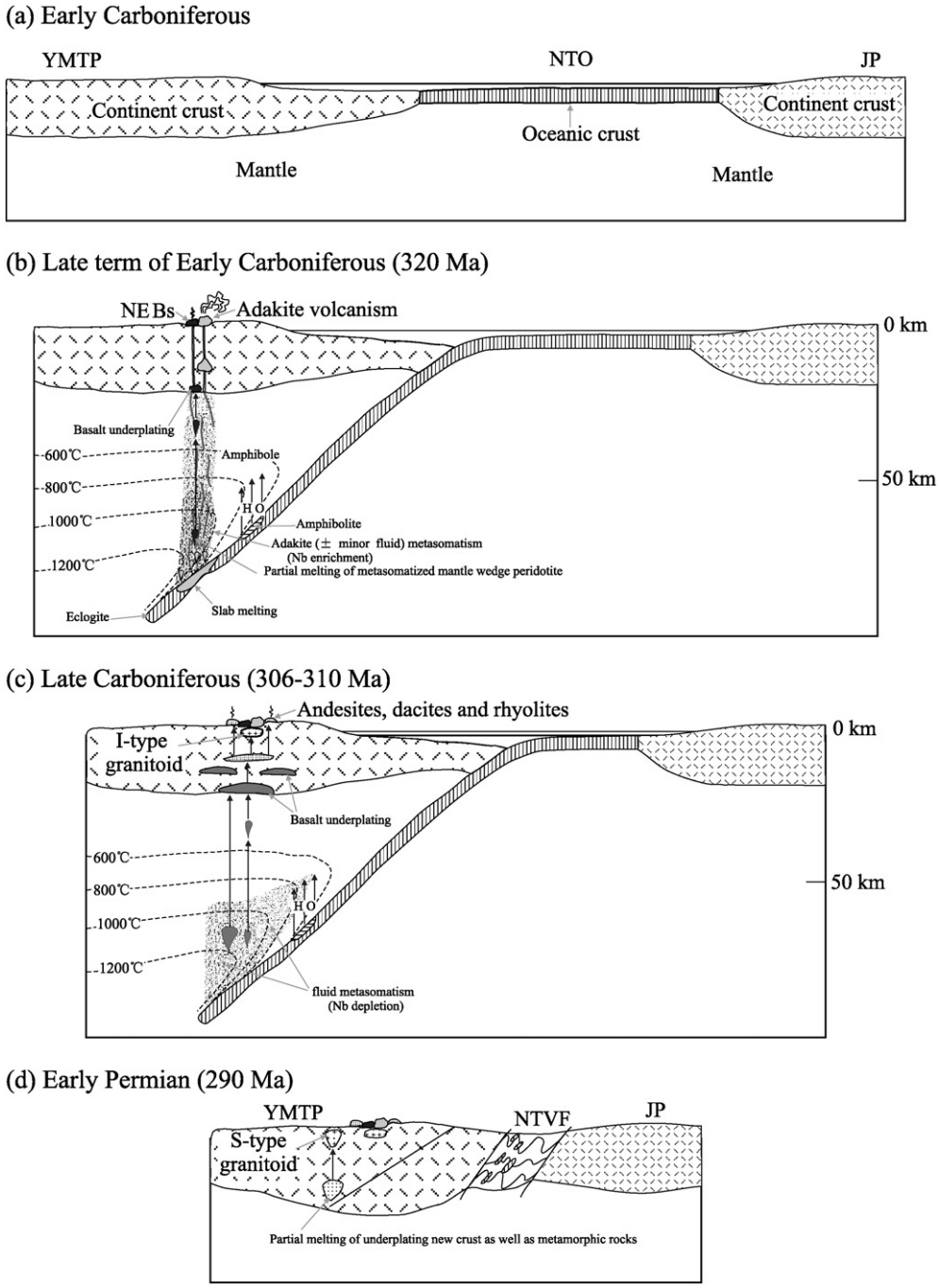

Fig. 13. A suggested model to produce the Late Paleozoic igneous rocks of the Alataw area. (a) Early Carboniferous: A Northern Tianshan Ocean existed between the Yili–middle-Tianshan microplate and Junggar plate. (b) Late–Early Carboniferous (320 Ma): Oceanic crust of the northern Tianshan ocean was subducted southwestward beneath the Yili–middle-Tianshan Plate. Both the dehydration and partial melting of subducted slab probably took place. The slab-derived adakitic magmas and aqueous fluids metasomatized or interacted with the mantle wedge peridotites. Partial melting of metasomatized mantle wedge peridotites generated Nb-enriched magmas. (c) Late Carboniferous (306–310 Ma): As subducted oceanic crust became older, slab dehydration began to dominate over slab melting resulting in widespread partial melting of mantle wedge peridotites and generation of basaltic magmas. Some of the basaltic magmas underplated the lower crust but AFC processes also lead to the formation of 'normal' andesites, dacites and rhyolites. (d) Early Permian (290 Ma): Collision between the Yili–middle-Tianshan microplate and Junggar plate caused the formation of the 'Syn-collision' S-type granitoids. JB—Junggar Plate; NTO—Northern Tianshan Ocean; NTVF—Northern Tianshan Variscan fold belt; YMTP—Yili–middle-Tianshan Plate.

mineral in the source. On the other hand, the slight concavity of the middle REE (7e) indicates that some residual hornblende probably remained in the source region (e.g., Gromet and Silver, 1987).

The large compositional range exhibited by the adakites also argues against genetic models that do not incorporate a role for mantle peridotites. Whereas some of the Alataw adakites have compositions similar to the experimental melts of metabasaltic and eclogite melts (1–4.0 GPa) and could conceivably be derived from lower crustal melts (e.g., Atherton and Petford, 1993; Petford and Atherton, 1996), the more magnesian adakites are similar to metabasaltic and eclogite melts hybridized by 10–16% peridotite (Fig. 12) and are inconsistent with the lower crustal melt model. Conversely, many workers, such as Bourdon et al. (2002) and Martin et al. (2005), have argued that some adakitic rocks may be generated by melting of mantle that has been metasomatised by slab melts. Martin et al. (2005) argue on the basis of a large data compilation that this mechanism of adakite formation can be distinguished from contamination of slab melts. For example, the low Cr/Ni ratios of wedge-derived "low silica-adakites" (SiO_2 generally 50 to 60 wt.%) reflect the composition of their peridotite source whereas the more variable Cr/Ni ratios of "high-silica adakites" correlate with Mg# because they are derived primarily from basaltic, subducted slab, sources (Fig. 10). Based on the criteria of Martin et al. (2005), the Alataw adakites have compositions that are consistent with a slab melt source that has been modified by interaction with the wedge (eg., $SiO_2 > 60$ wt.% and $TiO_2 < 0.7$ wt.% with Cr/Ni mostly greater than 1.5). In summary, the evidence suggests that moderate degrees of interaction between ascending slab-derived magmas and mantle wedge peridotites was responsible for generation of the Alataw adakites (e.g., Stern and Kilian, 1996; Rapp et al., 1999; Defant and Kepezhinskas, 2001; Martin et al., 2005).

5.2. Petrogenesis of NEBs

Two alternative mantle sources have been proposed to account for the origin and distinctive geochemical characteristics of NEB: (1) an OIB mantle or enriched mantle component occurring in the mantle wedge (e.g., Castillo et al., 2002); (2) a mantle wedge that was metasomatized by adakites (Defant et al., 1992; Defant and Drummond, 1993; Sajona et al., 1993, 1996; Kepezhinskas et al., 1996; Wyman et al., 2000; Aguillón-Robles et al., 2001; Defant and Kepezhinskas, 2001; Defant et al., 2002; Bourdon et al., 2002; Smithies et al., 2005). Partial melting of either of these two mantle sources plausibly generates NEBs. However, we consider that the latter mechanism likely played an important role in the petrogenesis of the Alataw NEBs. For example, rare adakite-metasomatized arc-mantle xenoliths have been identified and they are interpreted as the source of NEBs (e.g., Kepezhinskas et al., 1996; Defant et al., 2002). Similarly, Schiano et al. (1995) discovered pure adakitic glass inclusions in olivine crystals in mantle peridotite nodules from Batan Island and interpreted the inclusions as evidence for slab melt–peridotite interactions.

As observed by Defant et al. (1992) and Sajona et al. (1996), all the areas where Cenozoic NEBs occur have at least two common features: (1) they are underthrust by young (≤25 Ma) oceanic crust; and (2) adakites and NEBs are erupted more or less simultaneously. As noted above, the Alataw area was likely to have met both of these criteria in the Carboniferous while the large compositional range of the Alataw adakites also suggests interaction between slab melts and a mantle wedge. Given that Nb and Ti preferentially reside in melt within melt-fluid coexisting system, (e.g., $D^{fluid/melt}$ for Nb and Ti between fluid and andesitic melt are less than 0.004–0.005 and 0.005–0.026, respectively: Keppler, 1996), then slab melt metasomatism of the wedge would lead to the formation of Nb, Ti and Na_2O-rich amphibole and ilmenite, or amphibole and Fe-rich orthopyroxene (e.g., Sajona et al., 1993, 1996; Hollings and Kerrich, 2000; Polat and Kerrich, 2001). The NEBs derived from partial melting of the metasomatized mantle have much higher Nb and Ti contents than the "normal" arc basalt-basaltic andesite (Fig. 9).

The Alataw NEBs have varying $\varepsilon_{Nd}(T)$ (+6.4–+11.6) and $(^{87}Sr/^{86}Sr)_i$ (0.7007–0.7063) values, which indicates that either: (1) their source was compositionally heterogeneous or further changed by components other than adakites, which display relatively restricted $\varepsilon_{Nd}(T)$ values (+3.4–+6.6) and $(^{87}Sr/^{86}Sr)_i$ ratios (0.7035–0.7042) (Table 3 and Fig. 11); or (2) they underwent assimilation of old crustal materials which had low $\varepsilon_{Nd}(T)$ values and high $(^{87}Sr/^{86}Sr)_i$ ratios (Fig. 11). Similar to the CA (calc-alkaline) group NEBs in Philippines (Sajona et al., 1996), some Alataw NEBs samples exhibit slightly negative Nb and Ti anomalies (Fig. 7d). In Fig. 9b these NEBs define one of two trends characterized by nearly constant Nb/La at overlapping MgO contents. The results suggest that our NEB samples encompass two similar but distinct suites, which is also consistent with the isotopic variability found in these rock types.

The mechanism favoured for generation of the Alataw NEB resembles that proposed by Martin et al. (2005) for low-silica adakites (or magnesian basalts), but does not require the amphibole-enhanced stability of garnet cited by Martin et al. (2005) for the generation of low-silica

adakites. Nonetheless, the NEB defines a field that partially overlaps that of the wedge-derived adakites on their high-silica–low-silica adakite discrimination plots (Fig. 10).

In contrast to the NEB, the andesitic to rhyolitic Alataw high-K suite and coeval I-type granitoids exhibit the typical geochemical characteristics of arc magmatic rocks (Figs. 7a and b, 8, 9), which suggests that they originated from mantle wedge peridotite that had been metasomatized by subducting slab-derived aqueous fluids (e.g., Maury et al., 1992; Keppler, 1996) although some old crustal material must have played an important role in their petrogenesis, as suggested by the mass balance calculations of Chen et al. (2000b). In the context of the present study, the significance of high-K suite is that it provides evidence of subduction tectonics following eruption of the NEB and adakite suites. Moreover, any crustal thickening associated with emplacement of the I-type granitoids occurred after production of the adakite melts, which does not favour generation of these melts from deep or delaminated crust.

5.3. Geodynamic processes

The Tianshan Range extends east–west for at least 2500 km in central Asia and its tectonic evolution has been the subject of numerous studies (e.g., Sengör et al., 1993; Chen et al., 1999; Gao and Klemd, 2003). There is now a broad consensus that late Paleozoic sutures occur in both the southern and northern parts of the Tianshan Range (Fig. 1). Most researchers argue that the northern suture marked the Permian closure of an ocean between the Yili–middle-Tianshan microplate and Junggar plate (Windley et al., 1990; Zhao et al., 1990; Xiao et al., 1992; Hsü et al., 1994). The ocean had probably opened in the early Carboniferous and has been variously named the 'Carboniferous northern Tianshan ocean', 'Carboniferous Asian ocean' or 'early Carboniferous small oceanic basin' (e.g., Huang et al., 1990; Xiao et al., 1992; He et al., 1994; Zhao et al., 2003) (Fig. 13a). The age of the ocean has recently been confirmed by geochronological data for the Bayinggou ophiolites in the Northern Tianshan Variscan fold belt, as noted above (325± 7 Ma: Xu et al., 2006).

The petrogenesis of the Alataw adakites and NEB must be considered in the context of subduction-related ophiolites and high-K magmatism that pre-date and post-date their eruption. During the Early Carboniferous, oceanic crust of the northern Tianshan ocean subducted southwestward beneath the Yili–middle-Tianshan Plate, which resulted in a Carboniferous island arc in the northeastern margin of the Yili–middle-Tianshan Plate (Fig. 13b). The initiation of subduction, and the associated formation of ophiolites is associated with high thermal gradients (eg., Bloomer et al., 1995). As a consequence, the subducted slab soon reached its solidus temperature and melted to generate adakitic magmas (Martin, 1999). The slab-derived adakitic magmas, along with fluids liberated from the slab, metasomatized the mantle wedge peridotites during ascent, which triggered partial melting to generate NEB magmas (Fig. 13b) and the eruption of adakite-NEB suites. As subduction continued, the age of oceanic crust evidently increased, which promoted the release of fluids from the subducting oceanic crust rather than slab melting. Partial melting of mantle wedge peridotites generated large volumes of magma which was variably modified by the assimilation of crustal material during ascent. Combined with fractionation, this process resulted in the late Carboniferous calc alkaline to high-K calc alkaline volcanic and intrusive suite (Fig. 13c). This stage of magmatism resembled that found at centres such as Taupo and Mt. Taranaki (Egmont) in modern New Zealand (Price et al., 1999). Subduction ended in the Early Permian with the collision of the Yili–middle-Tianshan microplate and Junggar plate, which trigged partial melting in the crustal and generation of the 'Syn-collisional' S-type granitoids (Fig. 13d).

5.4. Implications for Phanerozoic crustal growth

Sengör et al. (1993) argued that nearly half of the CAOB was derived from the mantle by the formation of new crust during subduction processes. Nevertheless, many other investigations of voluminous Tianshan granites have suggested that they were related to massive underplating of basaltic magma, magmatic mixing, or AFC processes in an extensional continental setting (Chen et al., 2000b; Wang et al., 2004c). In these scenarios crustal growth was largely post-collision and vertical (e.g., Han et al., 1997; Jahn et al., 2000a,b; Wu et al., 2000, 2002). Zhou et al. (2004) argued that a Late Permian plume was likely responsible for the Huangshan mafic-ultramafic intrusive suite in the eastern Tianshan Range, for which they obtained an average $^{206}Pb/^{238}U$ age of 269±2 Ma by SHRIMP analysis of zircons in diorite. Irrespective of whether the Huangshan magmas were emplaced in response to a plume, Zhou et al. (2004) noted that their chemical and isotopic compositions require a subduction-modified component, which they infer to be metasomatised lithosphere. One important implication of their study is that the ~325 Ma to ~290 Ma sequence of ophiolite, adakite-NEB, high-K magmas and S-type granites described here could not have been linked to processes, such as crustal

delamination or rifting, that would have removed the subduction-modified lithosphere required to generate the younger Huangshan suite. Precise dating of granites in the CAOB (e.g., Hong et al., 1994; Heinhorst et al., 2000; Jahn et al., 2000a,b; Wu et al., 2000, 2002; Liu and Fei, 2006) shows they were generated over a time span encompassing 300–120 Ma (i.e., Permian–Cretaceous). Accordingly, lateral accretion processes must have dominated crustal growth in the CAOB prior to ~270 Ma (Sengör et al., 1993) but may have been augmented by vertical growth mechanisms after this date (e.g., Han et al., 1997; Jahn et al., 2000a,b; Wu et al., 2000, 2002; Liu and Fei, 2006).

6. Conclusions

This study has helped to clarify several important features of Carboniferous magmatism and tectonics in the Tianshan Range. The results also have major implications for the geodynamic development of the entire Central Asian orogenic belt. The principal findings are:

(1) Early Carboniferous adakites and NEBs in the Alataw area, Northern Tianshan Range, are part of a spectrum of subduction-related magmatism that began with ophiolites at ~325 Ma and ended with ~307 Ma high-K volcanism and granite plutonism followed by post-collisional S-type granites at 290 Ma.
(2) The Alataw adakites were derived by the partial melting of the subducting Northern Tianshan oceanic crust. The NEBs originated from mantle wedge peridotites metasomatized by adakites as well as minor slab-derived fluids. AFC processes also played a role in the petrogenesis of NEBs during magmas ascent. The dominantly high-K magmas of the area indicate a transition to typical subduction magmatism generated in response to fluid metasomatism of the mantle wedge.
(3) Crustal growth in the Central Asian orogenic belt was dominated by subduction-related processes until at least ~270 Ma and subduction modified material continued to be a volumetrically significant component of any later crustal additions.
(4) Some researchers suggest that Carboniferous volcanic rocks in other parts of the Tianshan Range were rift-related, based on "intraplate" geochemical characteristics of basaltic rocks in several areas (e.g., Luotuogou and Tuwu: Che et al., 1996; Xia et al., 2004a,b). However, we consider that these basalts are very similar to the Alataw NEBs, in terms of key criteria such as high TiO_2, P_2O_5 and Nb/La but low Nb/U ratios (Fig. 9). These basalts were most plausibly generated by subduction processes similar to those outlined here for the Alataw suite.

Acknowledgments

We thank editor Professor Roberta Rudnick, Professor Hervé Martin, and Drs. Erwan Bourdon and David Champion for their constructive and helpful reviews. This study was jointly supported by the Major State Basic Research Program of People's Republic of China (No. 2001CB409803), and the National Natural Science Foundation of China (Grant No. 40421303, 40673037, 40572042 and 40372041).

Appendix A. Supplementary data

Supplementary data associated with this article can be found, in the online version, at doi:10.1016/j.chemgeo.2006.08.013.

References

Aguillón-Robles, A., Caimus, T., Bellon, H., Maury, R.C., Cotton, J., Bourgois, J., Michaud, F., 2001. Late Miocene adakite and Nb-enriched basalts from Vizcaino Peninsula, Mexico: indicators of East Pacific Rise subduction below southern Baja California. Geology 29, 531–534.

Atherton, M.P., Petford, N., 1993. Generation of sodium-rich magmas from newly underplated basaltic crust. Nature 362, 144–146.

Bloomer, S.H., Taylor, B., MacLeod, C.J., Stern, R.J., Fryer, P., Hawkins, J.W., Johnson, L., 1995. Early arc volcanism and the ophiolite problem: a perspective from drilling in the western Pacific. AGU Geophys. Monogr. 88, 1–30.

Bourdon, E., Eissen, J.P., Monzier, M., Robin, C., Martin, H., Cotton, J., Hall, M.L., 2002. Adakite-like lavas from Antisana volcano (Ecuador): evidence for slab melt metasomatism beneath the Andean Northern volcanic zone. J. Petrol. 43, 199–217.

Bourdon, E., Eissen, J.P., Gutscher, M.A., Monzier, M., Hall, M.L., Cotton, J., 2003. Magmatic response to early aseismic ridge subduction: the Ecuadorian margin case (South America). Earth Planet. Sci. Lett. 205, 123–138.

Boynton, W.V., 1984. Cosmochemistry of the earth elements: meteorite studies. In: Henderson, R. (Ed.), Rare Earth Element Geochmistry: Developments in Geochemistry, vol. 2. Elsevier, Amsterdam, pp. 89–92.

Castillo, P.R., Janney, P.E., Solidum, R.U., 1999. Petrology and geochemistry of Camiguin island, southern Philippines: insights to the source of adakites and other lavas in a complex arc setting. Contrib. Mineral. Petrol. 134, 33–51.

Castillo, P.R., Solidum, R.U., Punongbayan, R.S., 2002. Origin of high field strength element enrichment in the Sulu Arc, southern Philippines, revisited. Geology 30, 707–710.

Che, Z.C., Liu, L., Liu, H.F., Luo, J.H., 1996. Review on the ancient Yili rift, Xinjiang, China. Acta Petrol. Sin. 12, 478–489 (in Chinese with English abstract).

Chen, J.F., Chen, D.G., Li, X.M., Zhou, T.X., Foland, K.A., 1994. K–Ar and $^{40}Ar/^{39}Ar$ geochronology of granites from the Alataw

Mountains, northwest Xinjiang, China. Acta Petrol. Sin. 10, 184–192 (in Chinese with English abstract).
Chen, C.M., Lu, H.F., Jia, D., Cai, D.S., Wu, S.M., 1999. Closing history of the southern Tianshan oceanic basin, western China: an oblique collisional orogeny. Tectonophysics 302, 23–40.
Chen, B., Jahn, B.M., Wilde, S., Xu, B., 2000a. Two contrasting paleozoic magmatic belts in northern Inner Mongolia, China: petrogenesis and tectonic implications. Tectonophysics 328, 157–182.
Chen, J.F., Zhou, T.X., Xie, Z., Zhang, X., Guo, X.S., 2000b. Formation of positive εNd (T) granitoids from the Alataw Mountains, Xinjiang, China, by mixing and fractional crystallization: implication for Phanerozoic crustal growth. Tectonophysics 328, 53–67.
Chung, S.L., Liu, D.Y., Ji, J.Q., Chu, M.F., Lee, H.Y., Wen, D.J., Lo, C.H., Lee, T.Y., Qian, Q., Zhang, Q., 2003. Adakites from continental collision zones: melting of thickened lower crust beneath southern Tibet. Geology 31, 1021–1024.
Coleman, R.G., 1989. Continental growth of northwest China. Tectonics 8, 621–635.
Condie, K.C., 2005. TTGs and adakites: are they both slab melts? Lithos 80, 33–44.
Dai, T.M., Hong, A.S., 1982. $^{40}Ar/^{39}Ar$ dating and some isotopic determinations on Himalaya biotites from granitoids rocks in southern Tibet. Geochimica 11, 48–55 (in Chinese with English abstract).
Defant, M.J., Drummond, M.S., 1990. Derivation of some modern arc magmas by melting of young subducted lithosphere. Nature 347, 662–665.
Defant, M.J., Drummond, M.S., 1993. Mount St. Helens: potential example of the partial melting of the subducted lithosphere in a volcanic arc. Geology 21, 547–550.
Defant, M.J., Kepezhinskas, P., 2001. Evidence suggests slab melting in arc magmas. EOS 82, 62–69.
Defant, M.J., Jackson, T.E., Drummond, M.S., De Boer, J.Z., Bellon, H., Feigenson, M.D., Maury, R.C., Stewart, R.H., 1992. The geochemistry of young volcanism throughout western Panama and southeastern Costa Rica: an overview. J. Geol. Soc. (Lond.) 149, 569–579.
Defant, M.J., Xu, J.F., Kepezhinskas, P., Wang, Q., Zhang, Q., Xiao, L., 2002. Adakites: some variations on a theme. Acta Petrol. Sin. 18, 129–142.
Gao, J., Klemd, R., 2003. Formation of HP-LT rocks and their tectonic implications in the western Tianshan Orogen, NW China: geochemical and age constraints. Lithos 66, 1–22.
Gao, S., Zhang, B., Gu, X., Xie, X., Gao, C., Guo, X., 1995. Silurian–Devonian provenance changes of South Qinling Basin: implications for accretion of the Yangtze (South China) to the North China Craton. Tectonophysics 250, 183–197.
Gao, S., Rudnick, R.L., Yuan, H.L., Liu, X.M., Liu, Y.S., Xu, W.L., Lin, W.L., Ayers, J., Wang, X.C., Wang, Q.H., 2004. Recycling lower continental crust in the North China craton. Nature 432, 892–897.
Gromet, L.P., Silver, L., 1987. REE variations across the peninsular ranges batholith: implications for batholithic petrogenesis and crustal growth in magmatic arcs. J. Petrol. 28, 75–125.
Gu, L.X., Hu, S.X., Yu, C.S., Li, H.Y., Xiao, X.J., Yan, Z.F., 2000. Carboniferous volcanites in the Bogda orogenic belt of eastern Tianshan: their tectonic implication. Acta Petrol. Sin. 16, 305–316 (in Chinese with English abstract).
Han, B.F., Wang, S.G., Jahn, B.M., Hong, D.W., Kagami, H., Sun, Y.L., 1997. Depleted-mantle magma source for the Ulungur River A-type granites from north Xinjiang, China: geochemistry and Nd–Sr isotopic evidence, and implication for Phanerozoic crustal growth. Chem. Geol. 138, 135–159.
He, G.Q., Li, M.S., Liu, D.Q., Tang, Y.L., Zhou, R.H., 1994. Paleozoic evolution and metallogenesis in Xinjiang, China. Wulumiqi: Xinjiang People's Publishing House and Hongkong, Educational and Cultural Press Ltd. 1– 437 (in Chinese with English abstract).
Heinhorst, J., Lehmann, B., Ermolov, V., Serykh, V., Zhurutin, S., 2000. Paleozoic crustal growth and metallogeny of Central Asia: evidence from magmatic-hydrothermal ore systems of Central Kazakhstan. Tectonophysics 328, 69–87.
Hollings, P., Kerrich, R., 2000. An Archean arc basalt–Nb-enriched basalt–adakite association: the 2.7 Ga confederation assemblage of the Birch–Uchi greenstion belt, Superior Province. Contrib. Mineral. Petrol. 139, 208–226.
Hong, D.W., Huang, H.Z., Xiao, Y.J., Xu, H.M., Jin, M.Y., 1994. The Permian alkaline granites in central inner Mongolia and their geodynamic significance. Acta Geol. Sin. 68, 219–230.
Hsü, K.J., Yao, Y.Y., Hao, J., Li, J.L., Wang, Q.C., 1994. Origin of Chinese Tianshan by arc–arc collision. Eclogae Geol. Helv. 87, 265–292.
Hu, A.Q., Jahn, B.M., Zhang, G.X., Chen, Y.B., Zhang, Q.F., 2000a. Crustal evolution and Phanerozoic crustal growth in northern Xinjiang: Nd isotopic evidence: part I. Isotopic characterization of basement rocks. Tectonophysics 328, 15–51.
Hu, S.H., Chen, A.F., Lin, S.L., Yuan, H.L., Gao, S., 2000b. ICP-MS analytical research into 40 trace and ultra-trace elements in geological samples (in Chinese with English abstract) Earth Sci. 25, 186–190.
Huang, J.Q., Jiang, C.F., Wang, Z.X., 1990. Plate tectonics and accordion-type movement. Xinjiang Geol. Sci. 1 (1), 3–16 (in Chinese).
Irvine, I.N., 1971. A guide to the chemical classification of the common vocanic rocks. Can. J. Earth Sci. 8, 532–548.
Jahn, B.M., Wu, F.Y., Chen, B., 2000a. Massive granitoid generation in Central Asia: Nd isotope evidence and implication for continental growth in the Phanerozoic. Episodes 23, 82–92.
Jahn, B.M., Griffin, W.L., Windley, B.F., 2000b. Continental growth in the Phanerozoic: evidence from Central Asia special issue. Tectonophysics 328, 1–227.
Johnson, K., Barnes, C.G., Miler, C.A., 1997. Petrology, geochemistry, and genesis of high-Al tonalite and trondhjemites of the Cornucopia stock, Blue Mountains, Northeastern Oregon. J. Petrol. 38, 1585–1611.
Kay, R.W., Kay, S.M., 1993. Delamination and delamination magmatism. Tectonophysics 219, 177–189.
Kay, R.W., Kay, S.M., 2002. Andean adakites: three ways to make them. Acta Petrol. Sin. 18, 303–311.
Kay, S.M., Ramos, V.A., Marquez, M., 1993. Evidence in Cerro Pampa volcanic rocks of slab melting prior to ridge trench collision in southern South America. J. Geol. 101, 703–714.
Kelemen, P.B., Yogodzinski, G.M., Scholl, D.W., 2003. Along strike variation in the Aleutian island arc: genesis of high-Mg# andesite and implications for continental crust. In: Eiler, J. (Ed.), Inside the Subduction Factory. Geophysical Monograph, American Geophysical Union, vol. 138, pp. 223–276.
Kepezhinskas, P.K., Defant, M.J., Drummond, M.S., 1996. Progressive enrichment of island arc mantle by melt-peridotite interaction inferred from Kamchatka xenoliths. Geochim. Cosmochim. Acta 60, 1217–1229.
Keppler, H., 1996. Constraints from partitioning experiments on the composition of subduction-zone fluids. Nature 380, 237–240.
Le Bas, M.J., Le Maitre, R.W., Streckeisen, A., Zanettin, B., 1986. A chemical classification of volcanic rocks based on the total alkali-silica diagram. J. Petrol. 27, 745–750.
Li, J.Y., Wang, K.Z., Li, W.Q., Guo, H.C., Song, B., Wang, Y., Mo, S.G., Zhao, Z.R., Zhu, Z.X., Pan, C.Z., 2002a. Tectonic evolution since the

Late Paleozoic and mineral prospecting in eastern Tianshan Mountains, NW China. Xinjiang Geol. 20, 295–301.

Li, X.H., Li, Z.X., Zhou, H.W., Liu, Y., Kinny, P.D., 2002b. U–Pb zircon geochronology, geochemistry and Nd isotopic study of Neoproterozoic bimodal volcanic rocks in the Kangdian Rift of south China: implications for the initial rifting of Rodinia. Precambrian Res. 113, 135–154.

Liu, W., 2002. Fluid–rock interaction during subsolidus microtextural development of alkali granite as exemplified by the Saertielieke pluton, Ulungur of the northern Xinjiang, China. Chem. Geol. 182, 473–482.

Liu, W., Fei, P.X., 2006. Methane-rich fluid inclusions from ophiolitic dunite and post-collisional mafic-ultramafic intrusion: The mantle dynamics underneath the Palaeo-Asian Ocean through to the post-collisional period. Earth Planet. Sci. Lett. 242, 286–301.

Man, F.S., 1990. Synthetical research report for the tungsten-Tin mineralization zone in the Bole area. National 305 Project Office of People's government of Xinjiang Uigur Municipality, Synthetical research of geology, geophysics and geochemistry for minerals and resources in Xinjiang area (sub-project IV_2), pp. 1–367.

Martin, H., 1999. Adakitic magmas: modern analogues of Archaean granitoids. Lithos 46, 411–429.

Martin, H., Smithies, R.H., Rapp, R., Moyen, J.F., Champion, D., 2005. An overview of adakite, tonalite–trondhjemite–granodiorite (TTG), and sanukitoid: relationships and some implications for crustal evolution. Lithos 79, 1–24.

Maury, R.C., Defant, M.J., Joron, J.L., 1992. Metasomatism of the sub-arc mantle inferred from trace elements in Philippine xenoliths. Nature 360, 661–663.

McCulloch, M.T., Chappell, B.W., 1982. Nd isotopic characteristics of S- and I-type granites. Earth Planet. Sci. Lett. 58, 51–64.

Muir, R.J., Weaver, S.D., Bradshaw, J.D., Eby, G.N., Evans, J.A., 1995. Geochemistry of the Cretaceous Separaton Plint Batholith, New Zealand: granitoid magmas formed by melting of mafic lithosphere. J. Geol. Soc. (Lond.) 152, 689–701.

Peccerillo, A., Taylor, S.R., 1976. Geochemistry of Eocene calc-alkaline volcanic rocks from the Kastamonu area, northern Turkey. Contrib. Mineral. Petrol. 58, 130–143.

Petford, N., Atherton, M., 1996. Na-rich partial melts from newly underplated basaltic crust: the Cordillera Blanca Batholith, Peru. J. Petrol. 37, 1491–1521.

Pfander, J.A., Jochurn, K.P., Kozakov, I., Kroner, A., Todt, W., 2002. Coupled evolution of back-arc and island arc-like mafic crust in the late-Neoproterozoic Agardagh Tes-Chem ophiolite, Central Asia: evidence from trace element and Sr–Nd–Pb isotope data. Contrib. Mineral. Petrol. 143, 154–174.

Plank, T., 2005. Constraints from thorium/lanthanum on sediment recycling at subduction zones and the evolution of the continents. J. Petrol. 46, 921–944.

Polat, A., Kerrich, R., 2001. Magnesian andesites, Nb-enriched basalt-andesites, and adakite from late-Archean 2.7 Ga Wawa greenstone belts, Superior Province, Canada: Implications for Late Archean subduction zone petrogenetic processes. Contrib. Mineral. Petrol. 141, 36–52.

Price, R.C., Stewart, R.B., Woodhead, J.D., Smith, I.E.M., 1999. Petrogenesis of high-K arc magmas: evidence from Egmont Volcano, North Island, New Zealand. J. Petrol. 40, 167–197.

Qin, K.Z., Sun, S., Li, J.L., Fang, T.H., Wang, S.L., Liu, W., 2002. Paleozoic epithermal Au and porphyry Cu deposits in North Xinjiang, China: epochs, features, tectonic linkage and exploration significance. Resour. Geol. 52, 291–300.

Rapp, R.P., Watson, E.B., 1995. Dehydration melting of metabasalt at 8–32 kbar: implications for continental growth and crust-mantle recycing. J. Petrol. 36, 891–931.

Rapp, R.P., Watson, E.B., Miller, C.F., 1991. Partial melting of amphibolite/eclogite and the origin of Archean trondhjemites and tonalites. Precambrian Res. 51, 1–25.

Rapp, R.P., Shimizu, N., Norman, M.D., Applegate, G.S., 1999. Reaction between slab-derived melts and peridotite in the mantle wedge: experimental constraints at 3.8 GPa. Chem. Geol. 160, 335–356.

Rapp, R.P., Xiao, L., Shimizu, N., 2002. Experimental constraints on the origin of potassium-rich adakite in East China. Acta Petrol. Sin. 18, 293–311.

Sajona, F.G., Maury, R.C., Bellon, H., Cotton, J., Defant, M.J., Pubellier, M., Rangin, C., 1993. Initiation of subduction and the generation of slab melts in western and eastern Mindanao, Philippines. Geology 21, 1007–1010.

Sajona, F.G., Maury, R.C., Bellon, H., Cotton, J., Defant, M., 1996. High field strength element enrichment of Pliocene–Pleistocene island arc basalts, Zamboanga Peninsula, western Mindanao (Philippines). J. Petrol. 37, 693–726.

Schiano, P., Clocchiatti, R., Shimuzu, N., Maury, R.C., Jochum, K.P., Hofmann, A.W., 1995. Hydrous, silica-rich melts in the sub-arc mantle and their relationship with erupted arc lavas. Nature 377, 595–600.

Sen, C., Dunn, T., 1994. Dehydration melting of a basaltic composition amphibolite at 1.5 and 2.0 GPa: implications for the origin of adakites. Contrib. Mineral. Petrol. 117, 394–409.

Sengör, A.M.C., Natal'in, B.A., Burtman, V.S., 1993. Evolution of the Altaid Tectonic Collage and Paleozoic crustal growth in Eurasia. Nature 364, 299–307.

Sigmarsson, O., Martin, H., Knowles, J., 1998. Melting of a subducting oceanic crust from U–Th disequilibria in Austral Andean lavas. Nature 394, 566–569.

Skjerlie, K.P., Patiño Douce, A.E., 2002. The fluid-absent partial melting of a zoisite-bearing quartz eclogite from 1.0 to 3.2 GPa: implications for melting in thickened continental crust and for subduction-zone processes. J. Petrol. 43, 291–314.

Smithies, R.H., Champion, D.C., Van Kranendonka, M.J., Howard, H.M., Hickman, A.H., 2005. Modern-style subduction processes in the Mesoarchaean: geochemical evidence from the 3.12 Ga Whundo intra-oceanic arc. Earth Planet. Sci. Lett. 23, 221–237.

Springer, W., Seck, H.A., 1997. Partial fusion of basic granulites at 5 to 15 kbar: implications for the origin of TTG magmas. Contrib. Mineral. Petrol. 127, 30–45.

Steiger, R.H., Jäger, E., 1977. Subcommission on geochronology: covention on the use of decay constants in geo- and cosmochronology. Earth Planet. Sci. Lett. 36, 359–362.

Stern, C.R., Kilian, R., 1996. Role of the subducted slab, mantle wedge and continental crust in the generation of adakites from the Austral Volcanic Zone. Contrib. Mineral. Petrol. 123, 263–281.

Sun, S.S., McDonough, W.F., 1989. Chemical and isotopic systematics of oceanic basalts: implications for mantle composition and processes. In: Saunders, A.D., Norry, M.J. (Eds.), Implications for Mantle Composition and Processes, Magmatism in the Ocean Basins. Geological Society Special Publication, vol. 42, pp. 313–345.

Wang, J.H., Yin, A., Harrison, T.M., Grove, M., Zhou, J.Y., Zhang, Y.Q., Xie, G.Y., 2003. Thermochronological constraints on two pulses of Cenozoic high-K magmatism in eastern Tibet. Sci. China, Ser. D 46, 719–729.

Wang, Q., Xu, J.F., Zhao, Z.H., Bao, Z.W., Xu, W., Xiong, X.L., 2004a. Cretaceous high-potassium intrusive rocks in the Yueshan–Hongzhen area of east China: adakites in an extensional tectonic regime within a continent. Geochem. J. 38, 417–434.

Wang, Q., Zhao, Z.H., Bao, Z.W., Xu, J.F., Liu, W., Li, C.F., Bai, Z.H., Xiong, X.L., 2004b. Geochemistry and petrogenesis of the Tongshankou and Yinzu adakitic intrusive rocks and the associated porphyry copper–molybdenum mineralization in Southeast Hubei, East China. Resour. Geol. 54, 137–152.

Wang, J.B., Wang, Y.W., Wang, L.J., 2004c. The Junggar Immature Continental Crust Province and its mineralization. Acta Geol. Sin. 78, 337–344.

Wang, Q., McDermott, F., Xu, J.F., Bellon, H., Zhu, Y.T., 2005. Cenozoic K-rich adakitic volcanic rocks in the Hohxil area, northern Tibet: lower-crustal melting in an intracontinental setting. Geology 33, 465–468.

Wang, Q., Xu, J.F., Jian, P., Bao, Z.W., Zhao, Z.H., Li, C.F., Xiong, X.L., Ma, J.L., 2006. Petrogenesis of adakitic porphyries in an extensional tectonic setting, Dexing, South China: implications for the genesis of porphyry copper mineralization. J. Petrol. 47, 119–144.

Windley, B.F., Allen, M.B., Zhang, C., Zhao, Z.Y., Wang, G.R., 1990. Paleozoic accretion and Cenozoic redeformation of the Chinese Tien Shan range, Central Asia. Geology 18, 128–131.

Winther, K.T., 1996. An experimentally based model for the origin of tonalitic and trondhjemitic melts. Chem. Geol. 127, 43–59.

Wu, F., Jahn, B., Wilde, S., Sun, D., 2000. Phanerozoic crustal growth: U–Pb and Sr–Nd isotopic evidence from the granites in northeastern China. Tectonophysics 328, 89–113.

Wu, F.Y., Sun, D.Y., Li, H.M., Jahn, B.M., Wilde, S., 2002. A-type granites in northeastern China: age and geochemical constraints on their petrogenesis. Chem. Geol. 187, 143–173.

Wyman, D.A., Ayer, J.A., Devaney, J.R., 2000. Niobium-enriched basalts from the Wabigoon subprovince, Canada: evidence for adakitic metasomatism above an Archean subduction zone. Earth Planet. Sci. Lett. 179, 21–30.

Xia, L.Q., Xia, Z.C., Xu, X.Y., Li, X.M., Ma, Z.P., Wang, L.S., 2004a. Carboniferous Tianshan igneous megaprovince and mantle plume. Geol. Bull. China 23, 903–910.

Xia, L.Q., Xu, X.Y., Xia, Z.C., Li, X.M., Ma, Z.P., Wang, L.S., 2004b. Petrogenesis of Carboniferous rift-related volcanic rocks in the Tianshan, northwestern China. Geol. Soc. Amer. Bull. 116, 419–433.

Xiao, X.C., Tang, Y.Q., Feng, Y.M., Zhu, B.Q., Li, J.Y., Zhao, M., 1992. Tectonic Evolution of the Northern Xinjiang and Its Adjacent Region. Geological Publishing House, Beijing, pp. 1–180 (in Chinese with English Abstract).

Xiao, W.J., Windley, B.F., Hao, J., Zhai, M.G., 2003. Accretion leading to collision and the Permian Solonker suture, inner Mongolier, China: termination of the Central Asian orogenic belt. Tectonics 22 (6), 1069, doi:10.1029/2002TC001484.

Xiong, X.L., Li, X.H., Xu, J.F., Li, W.X., Zhao, Z.H., Wang, Q., Chen, X.M., 2003. Extremely high-Na adakite-like magmas derived from alkali-rich basaltic underplate: the Late Cretaceous Zhantang andesites in the Huichang Basin, SE China. Geochem. J. 37, 233–252.

Xiong, X.L., Cai, Z.Y., Niu, H.C., Chen, Y.B., Wang, Q., Zhao, Z.H., Wu, J.H., 2005. The late Paleozoic adakites in eastern Tianshan area and their metallogenetic significance. Acta Petrol. Sin. 21 (3), 967–976 (in Chinese with English abstract).

Xu, J.F., Shinjio, R., Defant, M.J., Wang, Q., Rapp, R.P., 2002. Origin of Mesozoic adakitic intrusive rocks in the Ningzhen area of east China: partial melting of delaminated lower continental crust? Geology 30, 1111–1114.

Xu, J.F., Castillo, P.R., Chen, F.F., Niu, H.C., Yu, X.Y., Zhen, Z.P., 2003. Geochemistry of Late Paleozoic mafic igneous rocks from the Kuerti area, Xinjiang, Northwest China: implications for backarc mantle evolution. Chem. Geol. 193, 137–154.

Xu, X.Y., Xia, L.Q., Ma, Z.P., Wang, Y.B., Xia, Z.C., Li, X.M., Wang, L.S., 2006. SHRIMP zircon U–Pb geochronology of the plagiogranites from Bayinggou ophiolite in North Tianshan Mountains and the petrogenesis of the ophiolite. Acta Petrol. Sin. 22, 83–94 (in Chinese with English abstract).

Yogodzinski, G.M., Kay, R.W., Volynets, O.N., Koloskov, A.V., Kay, S.M., 1995. Magnesian andesite in the western Aleutian Komandorsky region: implications for slab melting and processes in the mantle wedge. Geol. Soc. Amer. Bull. 107, 505–519.

Zhang, Q., Qian, Q., Wang, E.C., Wang, Y., Zhao, T.P., Hao, J., Guo, G.J., 2001. Existance of East China Plateau in mid-late Yanshan period: implication from adakites. Sci. Geol. Sin. 36, 248–255 (in Chinese with English abstract).

Zhang, H.F., Sun, M., Zhou, X.H., 2002. Mesozoic lithosphere destruction beneath the North China Craton: evidence from major-, trace-element and Sr–Nd–Pb isotope studies of Fangcheng basalts. Contrib. Mineral. Petrol. 144, 241–253.

Zhang, L.C., Xiao, W.J., Qin, K.Z., Zhang, Q., 2006. The adakite connection of the Tuwu–Yandong copper porphyry belt, eastern Tianshan, NW China: trace element and Sr–Nd–Pb isotope geochemistry. Miner. Depos. 41, 188–200.

Zhao, X.X., Coe, R.S., Zhou, Y.X., Wu, H.R., Wang, J., 1990. New paleomagnetic results from northern China: collision and suturing with Siberia and Kazakhstan. Tectonophysics 181, 43–81.

Zhao, Z.H., Wang, Z.G., Zou, T.R., Masuda, A., 1996. Study on petrogenesis of alkali-rich intrusive rocks of Ulungur, Xinjiang. Geochimica 25, 205–220 (in Chinese with English Abstract).

Zhao, J.M., Liu, G.D., Lu, Z.X., Zhang, X.K., Zhao, G.Z., 2003. Lithospheric structure and dynamic processes of the Tianshan orogenic belt and the Junggar basin. Tectonophysics 376, 199–239.

Zhou, M.F., Robinson, P.T., Malpas, J., Aitchison, J., Sun, M., Bai, W.J., Hu, X.F., Yang, J.S., 2001. Melt/rock interaction and melt evolution in the Sartohay high-Al chromite deposit of the Dalabute ophiolite (NW China). J. Asian Earth Sci. 19, 519–536.

Zhou, M.F., Lesher, C.M., Yang, Z.Y., Li, J.W., Sun, M., 2004. Geochemistry and petrogenesis of 270 Ma Ni–Cu–(PGE) sulfide-bearing mafic intrusions in the Huangshan district, Eastern Xinjiang, Northwest China: implications for the tectonic evolution of the Central Asian orogenic belt. Chem. Geol. 209, 233–257.